NASA TM-86656

NASA Technical Memorandum 86656

Flow Visualization Study of a Vortex/Wing Interaction

R.D. Mehta and T.T. Lim

October 1984

NASA
National Aeronautics and
Space Administration

NASA Technical Memorandum 86656

Flow Visualization Study of a Vortex/Wing Interaction

R. D. Mehta,
T. T. Lim, Ames Research Center, Moffett Field, California

National Aeronautics and
Space Administration

Ames Research Center
Moffett Field, California 94035

NOMENCLATURE

c wing chord

d distance between vortex and wing-pivot point

Re $(=Uc/\nu)$ Reynolds number

U,V,W mean velocities in the streamwise, normal and spanwise directions, respectively

u,v,w fluctuating velocity components

α angle of attack of the main wing

α_g angle of attack of the vortex generator

Γ vortex circulation

SUMMARY

A flow visualization study in water has been completed on the interaction of a streamwise vortex with a laminar boundary layer on a two-dimensional wing. The vortex was generated at the tip of a finite wing at incidence, mounted perpendicular to the main wing, and having the same chord as the main wing. The Reynolds number based on wing chord was about 5×10^4. Two different visualization techniques were used. One involved the injection of two different colored dyes into the vortex and the boundary layer. The other technique utilized hydrogen bubbles as an indicator. In this study, the position of the vortex was varied in a direction normal to the wing. The angle of attack of the main wing was varied from -5° to +12.5°. It was found that the vortex induced noticeable cross flows in the wing boundary layer from a distance equivalent to 0.75 chords. When very close to the wing, the vortex entrained boundary layer fluid and caused a cross flow separation which resulted in a secondary vortex. In certain cases, two secondary vortices of opposite sign were induced and, in the right circumstances, asymmetric primary separation was also obtained on the main wing. The visual observations are also analyzed and discussed with respect to the critical point theory.

1. INTRODUCTION

Flows involving vortex interactions are often encountered in aerodynamics. It is well known that the interference of a streamwise vortex with a nearby lifting body, such as an aircraft wing, can have a strong effect on the aerodynamic characteristics of the wing. Apart from the obvious induced flow effects, a vortex can, if it is close enough, interact with and entrain the shear layers on the wing. These interactions are very complex and they often lead to drastic changes in the characteristics and performance of the wing which are difficult to predict. The complexity is due to the presence of three-dimensional viscous effects which must be fully understood if these interactions are to be modeled accurately. There are many practical situations in which this type of interaction is found. One particular example is on a rotorcraft, where a vortex generated by a blade-tip interferes with the boundary layer and wake of the trailing blade. Other examples are on aircraft where strakes or canard configurations produce vortices which interact with the shear layers on the main wing and body. In practice, the shear layers are almost always in a turbulent state which adds to the complexity since more sophisticated turbulence models would have to be developed before attempting to compute such interactions.

Over the years, several research efforts, both experimental and theoretical, have been directed towards a better understanding of this problem. Smith and Lazzeroni (1960) conducted investigations on the effect of a vortical wake on the aerodynamic characteristics of a finite-span rectangular wing. The theoretical methods they used included strip theory and reverse-flow theory, with and without a finite vortex core. The Prandtl lifting-line theory and the Weissinger theory were also used to calculate the spanwise distribution of vortex-induced loads. The reverse-flow theory adequately predicted the vortex interference lift and

Weissinger's theory predicted the spanwise variation of induced loads well. It was also found that the direction of vortex rotation affected the induced loads on the wing.

In a similar study, Patel and Hancock (1974) performed a series of experiments on the effect of a longitudinal vortex on a two-dimensional wing. Their investigation included a flow visualization study of the interaction using smoke and surface oil-flow techniques. Some surface pressure measurements, in the spanwise and streamwise directions were also made. They found that the overall trends of the induced loads could be determined by standard wing theory, but the detailed behavior of the load distributions could not be predicted adequately when the vortex was positioned very close to the wing surface. This was attributed to the presence of significant three-dimensional effects, including secondary separations in the wing boundary layer. When the vortex core impinged on the stagnation region, vortex breakdown was observed.

Ham (1974 and 1975) in some investigations on blade-vortex interactions found that the unsteady loading on the blade differed greatly from that predicted by lifting-surface theory. The measured pressure distributions suggested the presence of local flow separations which were attributed to the large (predicted) spanwise pressure gradients induced by the vortex. Using potential flow theory, Ham showed that the spanwise pressure gradient is proportional to the vortex circulation and inversely proportional to the airfoil-vortex spacing. He also derived a semiempirical relation for the maximum spanwise pressure gradient which was shown to be proportional to $\alpha_g^{2/3}$. His main conclusion was that consideration of the three-dimensional nature of the vortex-induced flow is essential when studying such interactions.

More recently, McAlister and Tung (1983) made a visual study of the vortex/wing interaction using hydrogen bubbles in a water tunnel. The vortex generator was located at two discrete positions, one along the center-line of the tunnel and the other at an offset distance equivalent to one-half the generator chord. The generator was set at three angles of attack (0°, 5°, and 10°) and the angle-of-attack of the main aerofoil was varied from -16° to +16°. Because of the limitations of their experimental set up, only side views of the interactions were studied. In addition to the visual study, measurements of the changes in the aerodynamic characteristics of the aerofoil, such as lift, drag and pitching moment were also made. They found that the vortex always caused premature stall, the stall angle being reduced by about 2°. Buffeting from a nearby separated region caused the vortex core to become unstable; when the vortex impinged on the stagnation region, vortex breakdown was observed. The results for the vortex trajectory and airfoil loads compared well with a theoretical model in the prestall regime. The theoretical model was a panel method formulation using Green's theorem.

It is apparent from the review given above that, although the vortex/wing interaction has received a lot of attention over the years, most of the efforts have concentrated on the measurement and prediction of the induced loads on the wing. The prediction methods do not perform well when the vortex lies very close to the wing surface, in which the viscous interaction between the vortex and the boundary layer produces a complex, three-dimensional flow field. No attempt has been made to study details of the shear layers on the main wing which must be adequately modeled if the performance of the wing is to be predicted accurately. The main objective of the present investigation was to study the effect of a longitudinal vortex on the boundary layer flow over a two-dimensional wing. In particular, the induced

three-dimensionality in the wing boundary layer was to be investigated in detail by studying the flow field from both the side- and plan-views. In the present study the relatively simpler case of a laminar boundary layer on the main wing was investigated. Future studies will be extended to the case of a turbulent boundary layer.

Section 2 contains details of the experimental apparatus and techniques. Results are presented in Section 3 and are discussed in relation to the critical point theory in Section 4. Section 5 contains the conclusions. A brief description of the critical point theory is given in appendix A.

2. EXPERIMENTAL APPARATUS AND TECHNIQUES

2.1 The Water Tunnel

The experiment was conducted in the NASA Ames-Dryden Water Tunnel. Figure 1 shows the general layout of the facility. The water tunnel is of a closed-return design with a vertical test section. The test section has a cross section of 41 x 61 cm (16 in. x 24 in.) and all four walls are constructed of Plexiglas, thus offering excellent visual access. There is no contraction section as such, but based on the area of the test section when compared to that of the entry section, the effective contraction ratio is about 5. The tunnel is driven by a centrifugal pump powered by a 50-hp ac motor. The volume flow rate of the water is controlled by a butterfly valve. The velocity in the test section can be varied from 0 to about 0.34 m/sec (1.1 ft/sec). There are three honeycombs installed in the tunnel, including one at the test section entry, for flow quality control. The models were mounted perpendicular to each other as shown in figures 2a and 2b, so as to minimize the wake effects of the generator.

2.2 Models

A NACA 0012 wing model was cast from a nonconducting fiber resin. The main wing had a 15-cm (6-in.) chord and a 41-cm (16-in.) span (fig. 3). The model had a stainless steel spar of 1.3-cm (0.5-in.) internal diam passing through the quarter-chord axis. This spar served two purposes; one to act as a support for the wing, and the other to provide passage for dye injection through a narrow slot on the surface of the model (fig. 3). The slot, 0.08 cm (0.031 in.) wide and 15 cm (6 in.) long was located at the quarter-chord location and aligned perpendicular to the direction of the flow. A platinum strip which was used as an electrode in the hydrogen-bubbles study was mounted flush with the surface at 1/12c and was spanned across the whole model.

A finite wing with the same profile shape (NACA 0012) was used as the vortex generator. The generator had a 15-cm chord and a 18-cm span. It was also supported by a 1.3-cm (0.5-in.) diam stainless steel spar passing through the quarter-chord axis. A 0.2-cm diam tubing was inserted through the spar and connected to the outlet tube at the generator tip for dye injection as shown in figure 2b.

2.3 Visualization Techniques

Two different visualization techniques were used; the first involved the injection of dyes into the flow and the second relied on the production of hydrogen bubbles.

To introduce dye on the surface of the model, the stainless steel tubing passing through the quarter-chord axis was connected to a dye reservoir. This reservoir had a unique facility for varying the pressure as well as the volume flow rate of the dye. To make the vortex visible, dye was injected at the tip of the vortex generator. In all the tests, care was taken to ensure that dye injection did not disturb the flow conditions significantly.

In the hydrogen bubble technique, the chemical process, electrolysis is used. The process is described by the following reaction formula:

$$2H_2O \rightarrow 2H_2 + O_2$$

To achieve the above chemical reaction, two electrodes are immersed in an electrolytic solution and a dc voltage is applied between them. During this process, hydrogen bubbles are formed at the cathode and oxygen bubbles are formed at the anode. Theoretically, both hydrogen and oxygen bubbles can be used for visualizing the flow. However, hydrogen bubbles are preferred since, for a given electrode diameter, their size is smaller than oxygen bubbles; thus, they would follow the actual flow patterns more precisely. Also, twice as many hydrogen bubbles are produced as oxygen bubbles.

In general, the size of the hydrogen bubbles generated depends on the following factors: (1) the size (diameter or width) of the electrode; (2) the electrical potential applied between the cathode and the anode; and (3) the electrical conductivity of the electrolyte.

For a general discussion of the above factors, and a detailed description of the hydrogen bubble technique, and its limitations, see the excellent article by Schraub et al. (1965); see also Merzkirch (1974) and McAlister and Carr (1978).

In the present study, a platinum strip on the model served as a cathode, and the anode was located some distance downstream. An electrode was also mounted on the vortex generator tip to inject bubbles into the vortex. Sodium sulfate was added to the water to increase its electrolytic conductivity.

2.4 Lighting and Photographic Techniques

Except for the hydrogen bubbles study where only a narrow sheet of continuous lighting was used to illuminate the flow, all the other visual records were obtained with the whole test section illuminated, by either continuous or flash sources of light. Continuous lighting was provided by two tungsten lamps which produced a total of 1 kW. Simultaneous still photographs were obtained from both, plan and end views and the movie sequences* were shot from an oblique angle covering both views.

---

*Mehta, R. D.; and Lim, T. T.: "Flow Visualization Study of a Vortex/Wing Interaction." 16 mm movie. Ames Phototechnology Branch Repository for copy.

2.5 Experimental Procedure

Throughout the present investigation, the vortex generator location was fixed at a distance of 91 cm (= 6-chord lengths) upstream of the wing (measured between pitch axis) and its angle of attack was set at 8.5°. This produced a vortex with a nondimensionalized circulation, Γ/Uc, of approximately 0.03. This circulation is an order of magnitude lower than that encountered on the actual helicopter blade tip. To minimize the effect of the generator wake on the wing, the generator was aligned perpendicular to the main wing. The angle of attack of the wing was varied from -5.0° to 12.5°. For each of these angles, the position of the vortex relative to the wing was varied from 0.75 c to approximately -0.15 c. In all the dye visual records, the streamwise vortex produced by the vortex generator was colored with red dye and the boundary layer material on the wing was colored with green dye. The sense of the vortex rotation was counterclockwise when viewed from downstream. The separation distance between the vortex and the wing, d, is defined as that between the end plane of the generator and the quarter-chord axis of the wing, which is also the pivot axis (fig. 2b). When the vortex is on the same side of the wing as the dye slot, d is defined positive.

3. RESULTS

3.1 Visualization Using Dyes

In this part of the study, the velocity in the test section was set at 0.34 m/sec (1.1 ft/sec). This resulted in a Reynolds number based on wing chord of about 50,000; the wing boundary layer was therefore expected to be in a laminar state.

When the flow was viewed from the side-view, the only indication of any vortex interaction was when the boundary layer material was lifted from the wing surface. Very little could be said about the influence of the vortex on the initial stability of the laminar boundary layer before the entrainment process began. In order to gain a better insight into the three-dimensional effects, simultaneous photographs in plan view and side view were obtained.

Figures 4a to 4d (see Plate I) show some simultaneous views of the flow interaction with $\alpha = -5°$. It is interesting to note that at $d = 0.75$ c; when viewed from the side (Plate I, fig. 4a), no significant effect is observed. However, in the plan view (Plate I, fig. 4b), the dye appears to have developed a slight deflection toward the right (recall the counterclockwise rotation of the vortex when viewed from downstream). This observed phenomenon could be explained in terms of the induced velocity that is imparted on the wing by the vortex. In addition, the dye injection on the down-going side of the vortex is also affected. This interference was due to the effects of transverse pressure gradients that were induced by the vortex; the induced pressure is higher on the down-going side of the vortex. At $d = 0.1$ c (Plate I, fig. 4c), the green dye can be seen to be lifting away from the wing surface and rotating around the vortex core, thus indicating entrainment of the boundary-layer material by the vortex. This could also indicate a secondary separation in the cross-stream plane. In the present analysis, separation in the cross-stream direction (with the separation line aligned streamwise) is defined as a secondary separation while that in the streamwise direction is defined as a primary separation. It is also apparent that the vortex follows a curved path into the

stagnation region before passing over the pressure surface of the wing. So in the absence of any external effects, the vortex seems to follow the free streamlines. Also, the cross flow and the region of influence on the dye outlet has increased (Plate I, fig. 4d). The diameter of the vortex increases as it passes over the wing and so the vorticity may have been reduced. In general, the vortex diameter will decrease as it accelerates over the airfoil before increasing as it decelerates into the wake (vortex stretching and compressing). It is not clear from these photographs as to what other secondary motions have been induced in the boundary layer. In this particular situation, it would be expected that the mean properties of the boundary layer are very much distorted.

More interesting events start to occur at the higher angles of attack. At $\alpha = 5°$ (Plate II, figs. 5a and 5b), streamwise (primary) boundary layer separation is induced by the vortex on the up-going side. At $d = 0.6$ c (Plate II, fig. 5a), the green dye is entrained upstream up to about 0.1 c by the recirculating flow near the surface. In addition, in the side-view, there is evidence of a shear layer instability indicated by the figure-like structures at the outer edge of the green dye. These shear layer vortices are normally a prerequisite to the transition process in a laminar shear layer. At $d = -0.1$ c (Plate II, fig. 5b), secondary separations in the cross flow are also evident.

These effects are more dramatic at $\alpha = 10°$ (Plates II and III, fig. 6a-d). At $d = 0.75$ c, the nature of the boundary layer appears to be transitional because of the presence of the shear layer vortices, but the flow on the wing is still attached and no cross-flow is apparent. An interesting flow behavior takes place when the vortex is very close to the wing, $d = -0.15$ c (Plate III, figs. 6c and 6d). The side view in figure 6c (Plate III) indicates primary boundary layer separation from the leading edge of the wing. However, as can be seen in the plan view (Plate III, fig. 6d), asymmetric separation occurs with the separation prominent only on the up-going side of the vortex. In this case, the wing would experience a very large rolling moment about the streamwise axis. The observed effect could be explained qualitatively by considering the effects of the vortex as an up wash and down wash. On the down-going side of the vortex, the down wash causes an effective decrease in the angle of attack of the wing. The opposite effect occurs on the up-going side. This effective change in the angle of attack is estimated to be about 2°. The estimate is based on results from the movie sequences which show that this airfoil stalled with separation from near the leading edge at $\alpha = 12.5°$. Also, previous data on the NACA 0012 airfoil performance suggests that this airfoil should stall at $\alpha = 12°$-$16°$ in this Reynolds number range. This interesting asymmetric phenomenon could obviously not be appreciated from the side view alone such as the one shown in figure 6c (Plate III). However, the side view does show a better perspective of the initial path of the vortex. There is also some indication of vortex shedding in the separated shear layer.

3.2 Visualization Using Hydrogen Bubbles

One of the main advantages of using the hydrogen bubble technique in this study was that the production of hydrogen bubbles on the main wing was not affected by the spanwise pressure gradients set up by the presence of the streamwise vortex in the close vicinity of the wing. Another advantage was that the hydrogen bubbles did not contaminate the water in the tunnel. They burst or "diffused" when passing through the pump and flow control devices. With the dyes, the water was found to be contaminated after about 30 min running, resulting in a blue tint which is apparent in some

of the dye photographs. Also, since the platinum electrode spanned the whole width of the wing, the extent of the effects discussed above could be examined in more detail. However, some problems were encountered with this technique.

In this technique, a lower velocity of 0.23 m/sec (0.75 ft/sec) was used. This gives a Reynolds number based on wing chord of about 3.7×10^4. This lower velocity was chosen to avoid contamination of the water caused by dirt and sediment, picked up from the floor of the tunnel, which resulted in a poor visual effect. It should be noted that this problem is not inherent to the hydrogen bubbles technique. A better filtering system in the tunnel would have solved the problem. In the present setup, it was not possible to run the filtering system on-line while the tunnel was in operation.

Figure 7 (Plate III) shows a plan-view of the vortex interacting with the wing boundary layer. Although the cross flow and entrainment effects are apparent, the details of the induced flow field are not as easily identified as in the dye photographs. The main observation from these tests was that the effects caused by the vortex (e.g., asymmetric primary separation) persist over the whole span of the wing, thus implying that the performance of the wing would be affected significantly by the presence of the vortex; it is not just a localized effect.

4. DISCUSSION

4.1 Cross Flow Effects

Several interesting features have emerged from these flow visualization results. One of the important findings was that the vortex induces cross flows in the wing boundary layer from a relatively long distance of 0.75 c. Patel and Hancock (1974) also report observing cross flows from a distance of 0.5 c. The cross flows are caused by the induced velocity field which seems to be strong enough to affect the boundary layer flow from that distance. Whereas it is difficult to assess the changes in boundary layer structure caused by the cross flows in the present study, some of the effects may be inferred from a related study by Mehta (1984). In an experimental investigation on the effect of a longitudinal vortex on a turbulent mixing layer, it was found that while the vortex induced strong cross flows in the mixing layer, the primary shear stress ($\overline{uv}$) was not significantly affected. However, the cross-stream shear stress ($\overline{uw}$) changed drastically owing to the induced effects of the vortex. So the effects of the vortex are to induce three-dimensionality in the mean flow and turbulence within a turbulent shear layer. Although the boundary layer on the main wing in the present study was laminar, it must be noted that in practice, the boundary layer will almost always be in a turbulent state, so the three-dimensional effects in the turbulence would also have to be modeled.

4.2 Secondary Separation

Associated with the induced cross flow on the wing surface would be an attendant suction peak beneath the vortex core (fig. 8). Thus the cross-stream boundary layer would have to negotiate an adverse pressure gradient once it has passed under the vortex. When the vortex is sufficiently close to the wing, the adverse pressure gradient can become strong enough to cause separation (secondary separation) which forms a secondary vortex of opposite sign to the main vortex. In Patel and Hancock's

(1974) investigation, the surface oil-flow patterns (shown schematically in fig. 8) clearly indicated the presence of the secondary separation. Harvey and Perry (1971) in their studies of the flow field produced by a trailing vortex in the vicinity of the ground, also observed the generation of a separation bubble. Figure 9 shows their interpretation of the generated flow field. They found that further downstream, the bubble grew rapidly to the point where it detached from the surface as a secondary vortex, fed by a vortex sheet from the separation point. They predicted that since the secondary vortex was not confined by a vortex sheet feeding the main core, it was free to rise and that under the influence of the stronger main vortex would eventually spiral around it. However, this spiraling was not observed in their experiments. In the present study, the lifting of the green dye, as seen in figure 4c, does suggest the presence of a secondary separation. However, there is no direct evidence of a secondary vortex. This may be partly due to problems of assessing the rotational sense of the lifted boundary layer fluid. This could only be observed clearly if end views were available, with the cross plane illuminated. Such a cross-plane view at the main wing trailing edge was obtained in a similar vortex/wing study in a water channel (Plate III, fig. 10). Visualization is by fluorescent dyes in water, excited by a laser-light sheet aligned vertically and parallel to the wing trailing edge. The vortex (rotating counterclockwise) is green and the wing upper-surface boundary-layer material is yellow. The presence of the secondary vortex of opposite sign is clearly indicated.

The conjectured cross-flow streamline patterns at the trailing edge for the case when the angle of attack of the wing is less than ±5° are shown in figure 11a-c. The important critical points are also clearly indicated. In fluid dynamics, a critical point is a point where the velocity is zero. In flow close to the surface, it is also a point of zero vorticity and, hence, zero skin friction. Further details of the critical point theory are given in appendix A. Separatices, which are trajectories that start from or end at the saddles, are also shown in heavy lines. They devide the flow field into distinct regions. In figure 11a, the main vortex is represented by a stable focus asymptoting to the core as the streamlines spiral in. Also shown in figures 11a and 11b are dye interfaces included to represent the boundary layer edge. For simplicity, the interface is shown to follow the streamline patterns. This representation is valid only in the mean or steady sense. Since the flow in the present investigation is unsteady, streakline patterns (dye traces in this case) do not correspond to streamline patterns. The relationship between the two is rather complex (Kline, 1965). In figure 11c, the main vortex is now closer to the wing and the resultant adverse pressure gradient has caused a local separation in the cross-flow boundary layer, as discussed previously. The location of the separation line in the cross plane is indicated by a half-saddle point, S_1 where the resultant vortex sheet rolls up to form a secondary vortex. Reattachment occurs at a half-saddle point, R_1. In this particular case, part of the dye is entrained into the main vortex and the rest spirals into the secondary vortex. This situation with the secondary separation is more clearly illustrated in the perspective view shown in figure 12a. The evolution of the vortex sheet at the separation line and the form of the reattachment surface are indicated more clearly in this sketch. The separation line is shown to terminate at a saddle on the leading edge while the reattachment line terminates at a node. Figure 12b shows the conjectured surface-flow pattern corresponding to figure 12a. The separation and reattachment lines appear as the familiar "herring-bone" pattern. Patel and Hancock (1974) observed this pattern in their oil flow studies. For separation, the trajectories converge toward the line and this is indicated by a collection of dye in the present experiment. For reattachment, the reverse occurs so that a reattachment line would be identified by an absence of dye.

4.3 Generation of a Focus

An interesting phenomenon occurs in the case where a separation line is already defined.

The longitudinal vortex affects both the spanwise and streamwise pressure distributions on the wing (Patel and Hancock, 1974). The effect of the vortex on the streamwise distribution is to impose a more severe adverse pressure gradient on the up-going side. In the present case, the effect of the asymmetric streamwise pressure gradient would be to distort the separation line locally. A distorted separation line is found to form a focus on the surface from which a secondary vortex lifts off. In a related study on the effects of a longitudinal vortex on a separated boundary layer (Mehta, unpublished results), surface oil-flow visualization results show the separation line forming a secondary vortex (fig. 13). Winkelmann (1982) in his studies of separation patterns on stalled airfoils of finite span also observed these vortical separations. These appear in his oil flow experiment as "mushroom"-shaped structures terminating with a focus on each side of the midspan. These foci are the locations where the secondary trailing vortices lift off the surface. In this case, the secondary flow generation was due to edge effects and was presumably due to wingtip vortices in particular.

A plausible conjecture derived from some unpublished analysis by Tobak and Lim suggests that a focus on the surface is associated with an absolute pressure minimum. This conjecture is assumed to be valid in the present analysis and it often forms the basis for our conjectured flow patterns. Note that the converse is not necessarily true since there must be a negative pressure threshold which has to be exceeded before a focus is generated.

4.4 Generation of Two Foci

The most intriguing situation takes place at $\alpha = 5°$ (Figs. 5a and 5b). This is probably a situation where a laminar leading edge separation bubble forms on the wing. The dye patterns indicate the presence of two secondary separation lines with a reattachment line in between them when the vortex is very close to the wing surface. From figure 14, taken from Patel and Hancock (1974), it is apparent that when the vortex lies very close to the wing, two pressure minima can occur in the spanwise direction.* Assuming that the streamwise pressure distribution only has one pressure minimum, this gives two absolute pressure minima which can lead to two foci on the surface. Patel and Hancock (1974) observed two "bubbles" on the surface near the leading edge in their oil-flow studies. Figure 14 includes a schematic of these bubbles which we believe actually represent foci. The conjectured surface flow patterns for this case are shown in figure 15a, with two secondary vortices of opposite sign. The pattern need not be as symmetric as the one shown in this figure. Unfortunately, Patel and Hancock do not comment on the signs of their secondary

*Although Patel and Hancock's results are for $\alpha = 0°$, they obtained a leading-edge separation bubble in the absence of the vortex, which implies that the wing must have been at an effective angle of attack. The wing had a Clark Y profile (flat lower surface, rounded upper surface) and we believe that the effective angle of attack was probably about 5° and so direct comparison with the present case is justified.

vortices.) The flow of green dye toward the wing leading edge in figure 5b is consistent with the pattern in figure 15a. The cross-sectional pattern for this case is shown in figure 15b. We have assumed throughout the present analysis that the sign indicated by the surface flow pattern is consistent with that of the vortex which emerges into the flow, although it should be noted that this is not a necessary condition to satisfy, especially when there are more than one separation line feeding into the focus. The two separation lines originating from the critical points S_1 and S_2 and the reattachment point, R_1 are clearly shown in this sketch (fig. 15b). The appearance of the secondary vortex with the same sign as the main vortex may be attributed to the adverse pressure gradient set up by the first induced vortex (fig. 14). Once the cross flow passes over the first induced vortex, there is a flow expansion and if the adverse pressure gradient associated with it is strong enough, this will lead to yet another separation, S_2 in figure 15b. Using a different approach, in some instability analysis of boundary-layer flows, Tobak (1973) found that a separation bubble when perturbed would also result in two similar-induced vortices of opposite sign. Tobak also suggests that the mechanism underlying the bubble plays a significant role in the nature of the flow in the vertical plane of symmetry upstream of a cylindrical protuberance (fig. 16).

4.5 Asymmetric Primary Separation

At higher angles of attack ($\alpha \sim 10°$), the adverse pressure gradient on the up-going side of the vortex can become strong enough to cause streamwise (primary) separation from the leading edge. This is exactly the case in figures 6c and 6d where leading edge separation is induced by the vortex on the up-going side while the flow on the down-going side remains attached. It was observed in the movie sequences that this asymmetric separation occurs only when the vortex core lies very close to the wing surface. In this case, while there may still be two pressure minima in the spanwise direction, there would only be a pressure minimum on the unstalled part of the wing in the streamwise direction. Therefore, only one absolute pressure minimum, and hence one focus, is obtained on the surface. Considering the flow pattern for $\alpha = 5°$-$10°$ (fig. 15b), the secondary vortex most likely to be eliminated at $\alpha = 10°$ would be the second induced vortex, the one with the same sign as the main vortex. In that case the cross-flow pattern would be the same as for $-5° < \alpha < 10°$ (fig. 11c). However, it has been observed that the sign of the surface vortex, at least, is the same as that of the main vortex; in figure 13 the surface vortex rotates in a clockwise direction as does the main vortex when viewed from downstream. In the present case, the main vortex rotates in a counterclockwise direction when viewed from downstream, and for consistency, so should the surface vortex (fig. 17a). To be consistent with the earlier assumption, the vortex lifting off from the surface must also bear the same sign. The cross-flow pattern would then resemble the one shown in figure 17b. For the case of $\alpha = 10°$, although it is feasible that only one secondary separation should occur, it is not clear as to which of the two conjectures, figure 11c or 17b, is correct. More data are required before this question can be resolved.

In the movie sequences for $\alpha = 10°$, the situation conjectured in figures 15a and 15b, with two separation lines and one reattachment line was also observed when the vortex was at $d \sim 0.2\ c$. However, as the vortex core approached the wing surface, the primary asymmetric separation conjectured in figures 17a and 17b was found to dominate the interaction.

4.6 Regions of Topology

The results discussed above are summarized in the topography of separations shown in figure 18. Contours of the number of secondary separations (cross-stream separations and foci) are plotted in this chart. The shapes of the contours are derived from all the data obtained in the present investigation plus some intuitive observations. For example, as $\alpha \to 15°$, the main wing would stall completely with leading edge separation and so the vortex cannot be expected to induce further secondary separations. Also, there would be no absolute pressure minimum since the streamwise pressure minimum is now eliminated.

When the vortex lies very close to the wing surface, at $-5° < \alpha < 5°$, a secondary separation in the cross-flow plane is induced which terminates at a saddle point on the wing leading edge (fig. 12). As α is increased to 5°-10°, a second vortex is induced in the cross-flow plane with the same sign as the main vortex. With a laminar separation bubble near the leading edge, the two secondary vortices are found to evolve from foci on the surface (fig. 15). At $\alpha = 10°$, the vortex induces asymmetric primary separation with the wing stalled completely on the up-going side of the vortex. The separation in this case is a secondary vortex which evolves from one focus on the surface (fig. 17). At very high angles of attack ($\alpha > 15°$), the wing stalls completely with leading edge separation and the effects caused by the vortex will be minimal.

Patel and Hancock's (1974) results compare well with the conjectured topography. For $\alpha \sim 5°$, which is our estimate of the effective angle of attack in their test, they obtain no separations at $d/c = 0.5$, one secondary separation at $d/c = 0.2$ and two at $d/c = 0$. While the exact boundaries in the present chart obviously need refinement, the overall trends seem plausible.

4.7 Vortex Path

The present results seem to indicate that, overall, the vortex follows the "no-vortex" streamline path, implying that the vortex does not perturb the streamlines significantly. However, McAlister and Tung (1983) observed that for $\alpha = 8°$ the vortex in fact cuts across the no-vortex streamline path, moving in-board as it approached the wing. However, for $\alpha = -8°$, they found that the vortex was driven away from the surface. This was also observed in some cases in the present study (fig. 4c). As Harvey and Perry (1971) noted, this could be due to the influence of the secondary vortex which induces a normal velocity away from the surface on the main vortex. This is similar to the effect in a pair of vortices with the common flow moving away from the surface, where each vortex induces a normal velocity on the other (Mehta et al., 1983). This results in the pair moving away from the surface as it travels downstream.

4.8 Vortex Stability

Patel and Hancock (1974) and McAlister and Tung (1983) both report vortex breakdown under certain circumstances, normally when the vortex impinges on the stagnation region. The form of the breakdown is a helical distortion with a spiraling out of vorticity from a stagnation point. This type of vortex breakdown can occur under the influence of sudden, strong adverse pressure gradients such as those encountered when crossing a strong shock wave (Delery and Horowitz, 1983). However, it is not clear

if the adverse pressure gradient in the stagnation region alone is enough to cause vortex breakdown. McAlister and Tung (1983) also report vortex instability and breakdown because of the effects of the separated shear layer from the main wing. In the present study, whereas a reduction of vorticity was noted, mainly by observing the increase in the core diameter, the instability in the core was not obvious. It should be noted that in the other studies discussed above, the smoke or hydrogen bubbles were injected in a way so that, on the whole, only the core region of the vortex was visible. Therefore, it was easier to observe the detailed behavior of the core. In the present investigation, a greater part of the vortex was seeded and the detailed motions of the vortex core could therefore not be studied.

5. CONCLUSIONS

The results of this investigation clearly show that a longitudinal vortex has significant effects on the boundary layer flow on a two-dimensional wing. In practice, the vortex circulation would be about ten times higher and so the effects observed here would be greatly amplified. When the vortex core lies very close to the wing surface, very complex, three-dimensional secondary flows are induced in the boundary layer. The details of the effects (observed and conjectured) are found to fall into roughly three categories, defined by the angle of attack of the main wing.

For $-5° < \alpha < 5°$, the vortex induces cross flows in the wing boundary layer from a distance as far as 0.75 c. This may imply large structural changes in the boundary layer. When the vortex is positioned closer to the wing ($d \sim 0.1$ c), boundary layer material is lifted from the surface and a secondary separation is produced. Some of the boundary layer material was often seen to rotate around the vortex. This rotation dominates the interaction when the vortex core lies very close to the surface.

For $5° < \alpha < 10°$, the vortex induces streamwise separation on the up-going side from a distance of about 0.5 c. When the vortex core lies very close to the surface, a complex interaction produces two secondary vortices of opposite sign with two secondary-separation lines and a reattachment line in between.

The most dramatic effect occurs for $\alpha = 10°$. At $d \sim 0.2$ c, the same effects discussed above with two secondary vortices also seem to occur in this case. However, when the vortex core is very close to the surface, an asymmetric separation is produced with leading edge primary separation on the up-going side of the vortex. This flow field is conjectured as containing one secondary vortex which originates from a focus on the surface and bears the same sign as the main vortex.

The vortex seems to follow the no-vortex streamlines except when it is very close to the wing (-0.1 c $< d <$ 0.1 c) when viscous interactions start to dominate. The vortex strength and stability are found to be affected the most in the stagnation region of the wing.

ACKNOWLEDGMENTS

We would like to acknowledge the help of the staff at the NASA Ames-Dryden Research Center, in particular David Lux, Tony Ronquillo, Duane Hanson, and Carl Barnes. We are also grateful to Murray Tobak of NASA Ames Research Center for many helpful discussions, and to Tobak, Kenneth McAlister, and Chee Tung for comments on an earlier draft of this paper. We would like to thank Blair McLachlan for allowing us to use his unpublished results.

APPENDIX A

CRITICAL-POINT OR SINGULAR-POINT THEORY

This section outlines some of the basic concepts of the critical-point theory which we have used in interpreting the flow visualization results. The main purpose of this section is to familiarize the reader with some of the terminology which is used in the discussion in section 4. Critical-point theory (also known as "phase plane" or "phase space" method) has been used for a long time in examining the solutions of ordinary differential equations, and has proved to be highly successful in the field of nonlinear dynamical systems. Only recently has this method of approach been extended to the study of fluid flow. The mathematics is equivalent to the phase plane trajectory analysis, where solution trajectories on a phase plane can be thought of as instantaneous streamlines. The analysis involves the location of critical or singular points. By linearizing about them and examining other topological features of the solution trajectories, the most important features of the solution of a given differential equation set can be displayed in a descriptive manner. In complex, three-dimensional flow situations, the location of critical points cannot always be predicted analytically. However, the application of the resulting kinematic principles enables one to explore the type of critical points which are likely to occur, and this would help in deducing complicated streamline patterns from experimental results obtained in the wind tunnel.

In their review article, Tobak and Peake (1982) singled out the hypothesis proposed by Legendre (1956) as being one capable of providing a mathematical framework of considerable depth. Legendre proposed that a pattern of streamlines immediately adjacent to the surface be considered as trajectories having properties consistent with those of a continuous vector field. Oswatitch (1958) and Lighthill (1963) examined viscous flow patterns close to a rigid boundary and classified certain types of critical points (Legendre, 1965). Perry and Fairlie (1974) applied the phase plane trajectory analysis to the problem of viscous flow, and extended the approach to inviscid rotational flow with the slip condition applied at the boundaries. Various types of critical points were classified for this inviscid flow. Hunt et al. (1978) introduced the Poincaré Bendixson theorem, and with the aid of kinematic principles and theorems made studies of flow around obstacles. Tobak and Peake (1982) applied the theory to their study of skin friction patterns on bodies of various geometries. They also introduced the concept of structural stability and bifurcation theory. Cantwell et al. (1978) used it in their investigation of the geometry of turbulent spots. Perry and Lim (1978), Lim (1979), and Perry and Watmuff (1981) employed the theory to examine three dimensional flows. Further contributions to the extension and development of the theory can be found in Perry, Lim and Chong (1980), Hornung and Perry (1982), and in a recent article by Dallmann (1983). Detailed description of the basic theory involving phase plane method can be found in Andronow and Chaikin (1949), Kaplan (1958), Davis (1962), and Minorsky (1962).

In the following analysis, we will restrict our discussion to the phase plane or two-dimensional trajectories. It is to be noted that the same procedure can be extended to three dimensions.

Consider any set of autonomous differential equations (in which time does not appear explicitly) of the form:

$$dx/dt = \dot{x} = P(x,y)$$

$$dy/dt = \dot{y} = Q(x,y)$$

where in general P and Q are some nonlinear functions. Since time does not appear explicitly, the above equations can be arranged thus:

$$\dot{y}/\dot{x} = Q(x,y)/P(x,y)$$

For more information, see Kaplan (1958). The solution of the equations can be represented by

$$f(x,y) = 0$$

or

$$x = x(t) , \quad y = y(t)$$

In general, the solutions are unique; that is, for a given initial condition, there is only one trajectory passing through a point in the phase plane formed by x and y. However, there may exist certain points where both P(x,y) and Q(x,y) become zero simultaneously. Such a point is called a critical point. At such a point, the slope of the trajectory is indeterminate and the trajectories are allowed to cross.

To study the characteristics of the critical point, the origin of the coordinate system xy is placed at that point. Therefore, in region close to the singularity, the second- and higher-order terms in the equation may be neglected. This is the "first degree approximation" of Liaponov. The equations then become

$$\dot{y}/\dot{x} = Q(x,y)/P(x,y) = (cx + dy)/(ax + by)$$

where a, b, c, and d are constants which are in the governing nonlinear differential equations, Hence,

$$\begin{bmatrix} \dot{x} \\ \dot{y} \end{bmatrix} = \begin{bmatrix} a & b \\ c & d \end{bmatrix} \begin{bmatrix} x \\ y \end{bmatrix}$$

or

$$\underset{\sim}{\dot{x}} = [F] \underset{\sim}{x}$$

The matrix [F] is called the Jacobian, and in general will have two eigenvalues, λ_1 and λ_2, which may be real or complex conjugate. The corresponding eigenvector slopes are:

$$m_1 = (\lambda_1 - a)/b = c/(\lambda_1 - d)$$

$$m_2 = (\lambda_2 - a)/b = c/(\lambda_2 - d)$$

This leads to the classification of possible critical points which may be represented on a p - q chart as shown in figure A.1 where

$$p = -(a + d) = -\text{trace } F$$

$$q = (ad - bc) = \det F$$

and

$$\lambda_{1,2} = -1/2[p \pm (p^2 - 4q)^{1/2}]$$

In figure A.1, the critical points shown are called regular critical points. By the terms "stable" or "unstable," we simply mean that the direction of the flow is toward or away from the critical point respectively. No relationship with hydrodynamic stability is implied here. There also exists a certain class of critical points which correspond to values of p and/or q along the axes (i.e., $p = 0$ or $q = 0$) and on the parabola $p^2 = 4q$. These are called degenerate critical points and are shown in figure A.2 where the Roman numerals correspond to those on the $p - q$ chart shown in figure A.1.

In general, these critical points are expressed in noncanonical form (i.e., the eigenvectors are not orthogonal and not aligned with the coordinate axes). The equations for the trajectories are given by

$$(ax + by - \lambda_2 x) = K_1(ax + by + \lambda_1 x)^{\lambda_1/\lambda_2}$$

for

$$\lambda_1 \neq \lambda_2$$

and

$$\log K_2(ax + by - \lambda x) = \frac{\lambda x}{(ax + by - \lambda x)}$$

for

$$\lambda_1 = \lambda_2 = \lambda$$

where K_1 and K_2 are constants (detailed analysis is given by Davis, 1962). However, by some suitable affine transformation these trajectories can always be described in canonical form. It can be shown that with these transformations (Minorsky, 1962), the trajectory equations can be reduced to either simple power laws or logarithmic spirals depending on whether the eigenvalues are real or complex conjugates respectively. Figure A.3 shows a typical phase plane portrait of a node and a focus when plotted both in canonical and noncanonical form.

REFERENCES

Andronow, A. A.; and Chaikin, C. E.: Theory of Oscillations. Princeton University Press, 1949.

Cantwell, B. J.; Coles, D.; and Dimotakis, P.: Structure and Entrainment in the Plane of Symmetry of a Turbulent Spot. J. Fluid Mech., vol. 87, part 4, 1978, pp. 641-672.

Dallmann, U.: Topological Structures of Three-Dimensional Vortex Flow Separation. AIAA Paper 83-1735, June 1983.

Davis, H. T.: Introduction to Nonlinear Differential and Integral Equations. Dover Publication Inc., 1962.

Delery, J.; and Horowitz, E.: Interaction Entre Une Onde de Choc et une Structure Tourbillonnaire. AGARD-CP-342, 1982.

Ham, N. D.: Some Preliminary Results from an Investigation of Blade-Vortex Interaction. AHS J., vol. 19, no. 2, April 1974, pp. 45-48.

Ham, N. D.: Some Conclusions from an Investigation of Blade-Vortex Interaction. AHS J., vol. 20, no. 4, October 1975, pp. 26-31.

Harvey, J. K.; and Perry, F. J.: Flowfield Produced by Trailing Vortices in the Vicinity of the Ground. AIAA J., vol. 9, no. 8, 1971, pp. 1659-1660.

Hornung, H.; and Perry, A. E.: Streamsurface Bifurcation, Vortex Skeletons and Separation. DFVLR-IB Report 222-82 A-25, 1982.

Hunt, J. C. R.; Abell, C. J.; Peterka, J. A.; and Woo, H.: Kinematical Studies of the Flows Around Free or Surface-Mounted Obstacles; Applying Topology to Flow Visualization. J. Fluid Mech., vol. 86, part 1, 1978, pp. 179-200.

Kaplan, W.: Ordinary Differential Equations. Addison-Wesley Publishing Co., 1958.

Kline, S. J.: Pathlines, Streaklines and Streamlines in Unsteady Flow. FM-48 film loop. Nat. Com. Fluid Mech. Films.

Legendre, R.: Séparation de l'écoulement laminaire tridimensionnel. Rech. Aéro. vol. 54, 1956, pp. 3-8.

Legendre, R.: Lignes de courant d'un écoulement continu. Rech. Aérosp., vol. 105, 1965, pp. 3-9.

Lighthill, M. J.: In Laminar Boundary Layers (ed. L. Rosenhead). Oxford University Press: Clarendon Press, 1963.

Lim, T. T.: Coherent Structures in Coflowing Jets and Wakes. Ph.D. Thesis, Univ. of Melbourne, 1979.

McAlister, K. W.; and Carr, L. W.: Water-Tunnel Experiments on an Oscillating Airfoil at Re = 21,000. NASA TM-78446, 1978.

McAlister, K. W.; and Tung, C.: Airfoil Interaction With Impinging Vortex. NASA TP-2273, 1983.

Mehta, R. D.; Shabaka, I. M. M. A.; Shibl, A.; and Bradshaw, P.: Longitudinal Vortices Imbedded in Turbulent Boundary Layers. AIAA Paper 83-0378, Jan. 1983.

Mehta, R. D.: An Experimental Study of a Vortex/Mixing Layer Interaction. AIAA Paper 84-1543, June 1984.

Merzkirch, W.: Flow Visualization. Academic Press Inc., 1974.

Minorsky, N.: Nonlinear Oscillations. D. Van Nostrand Company Inc., 1962.

Oswatitsch, K.: Die Ablosebedingung von Grenzachichten, IUTAM Symposium on Boundary Layer Research, Freiburg, 1957.

Patel, M. H.; and Hancock, G. J.: Some Experimental Results of the Effect of a Streamwise Vortex on a Two-Dimensional Wing. Aero. J., vol. 78, no. 760, April 1974, pp. 151-155.

Perry, A. E.; and Fairlie, B. D.: Critical Points of Flow Patterns, Advances in Geophysics. Academic Press, 1974.

Perry, A. E.; and Lim, T. T.: Coherent Structures in Co-flowing Jets and Wakes. J. Fluid Mech., vol. 88, 1978, pp. 451-464.

Perry, A. E.; Lim, T. T.; and Chong, M. S.: The Instantaneous Velocity Fields of Coherent Structures in Coflowing Jets and Wakes. J. Fluid Mech., vol. 101, part 2, 1980, pp. 243-256.

Perry, A. E.; and Watmuff, J. H.: The Phase-Averaged Large-Scale Structures in Three-Dimensional Turbulent Wakes. J. Fluid Mech., vol. 103, 1981, pp. 33-51.

Schraub, F. A.; Kline, S. J.; Henry, J.; Runstadler, P. W.; and Littell, A.: Use of Hydrogen Bubbles for Qualitative Determination of Time-Dependent Velocity Fields in Low-Speed Water Flows. ASME J. Basic Eng., vol. 87, series D, no. 2, June 1965, pp. 429-444.

Smith, W. G.; and Lazzeroni, F. A.: Experimental and Theoretical Study of a Rectangular Wing in a Vortical Wake at Low Speed. NASA TN D-339, 1960.

Thwaites, B. (ed.): Incompressible Aerodynamics. Clarendon, Oxford, 1960.

Tobak, M.: and Peake, D. J.: Topology of Three-Dimensional Separated Flows. Ann. Rev. Fluid Mech., vol. 14, 1982, pp. 61-85.

Tobak, M.: On Local Inflexional Instability in Boundary-Layer Flows. ZAMP, vol. 24, 1973, p. 330-354.

Winkelmann, A. E.: An Experimental Study of Mushroom Shaped Stall Cells. AIAA Paper 82-0942, June 1982.

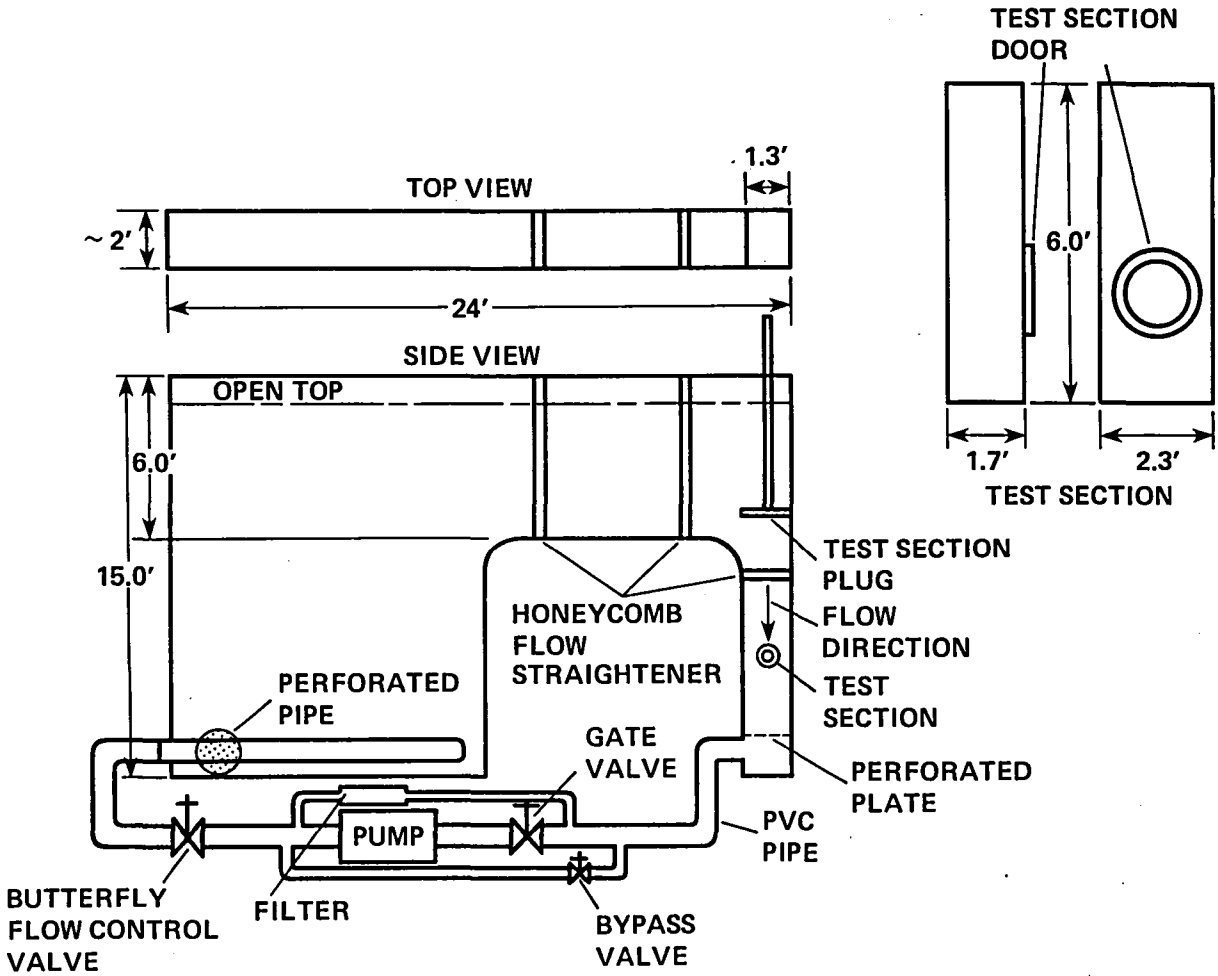

Figure 1.- Layout of NASA Ames-Dryden Water Tunnel.

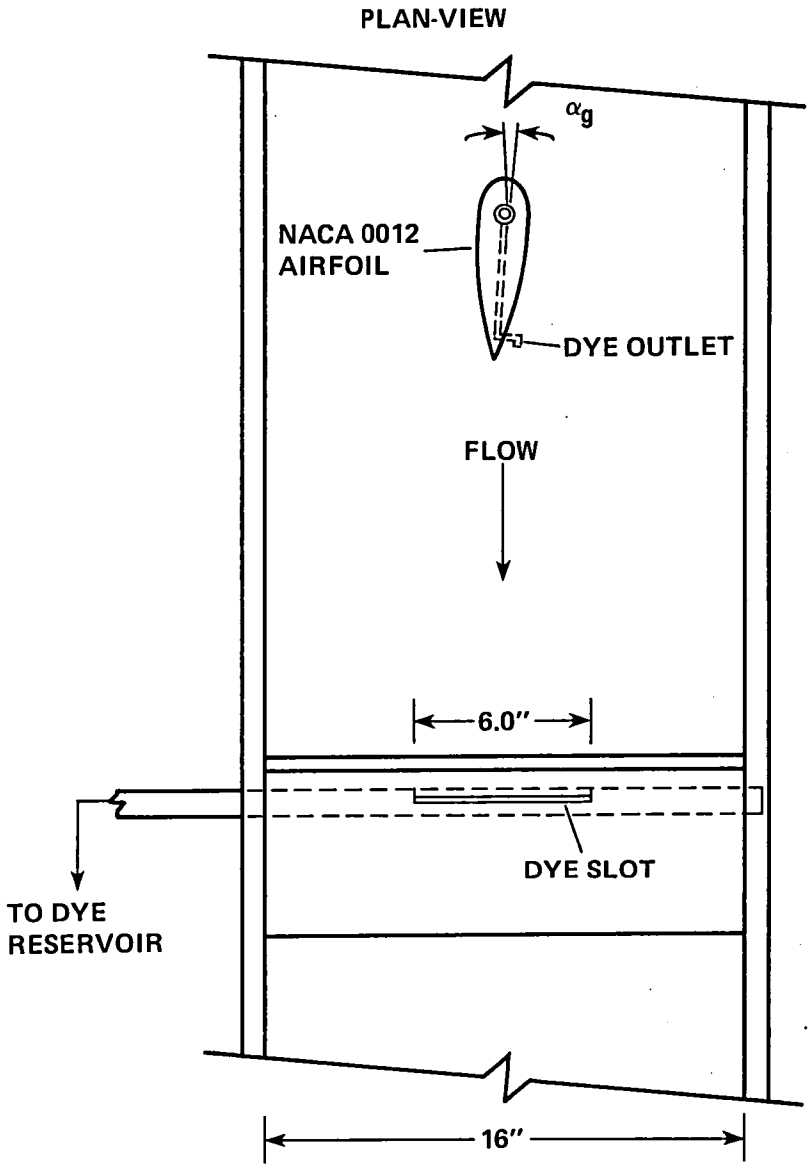

(a) Plan view.

Figure 2.- Schematic of model arrangement.

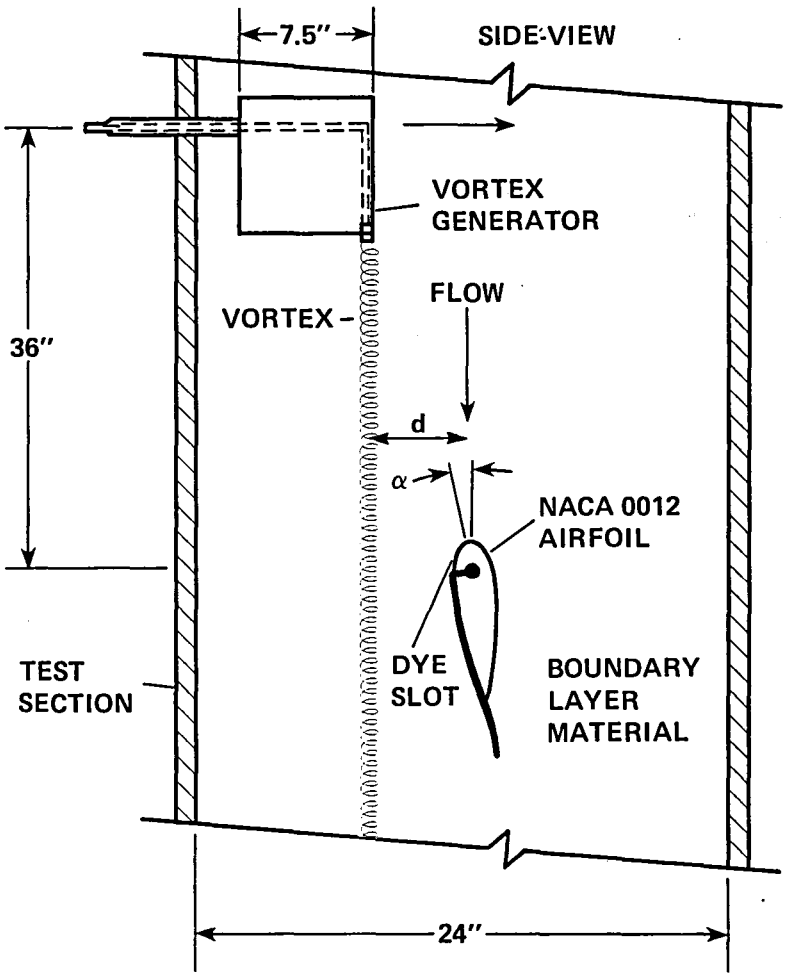

(b) Side view.

Figure 2.- Concluded.

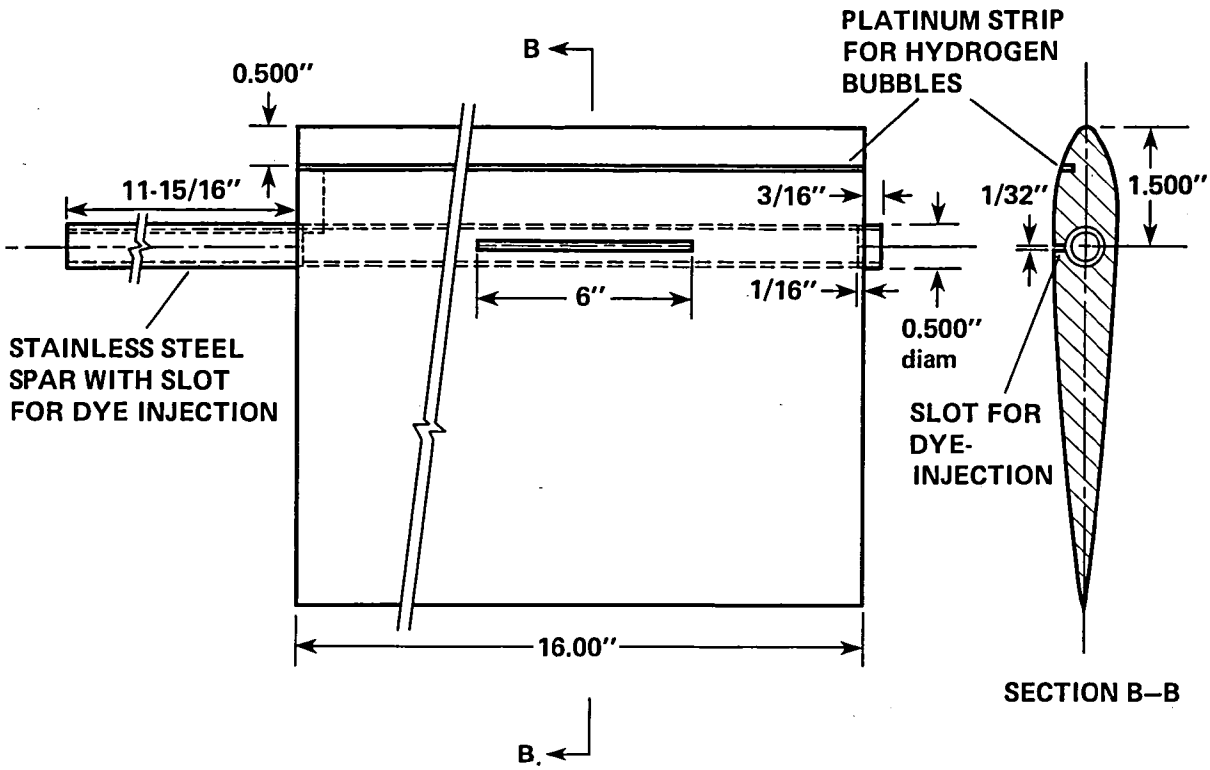

Figure 3.- Details of main airfoil construction.

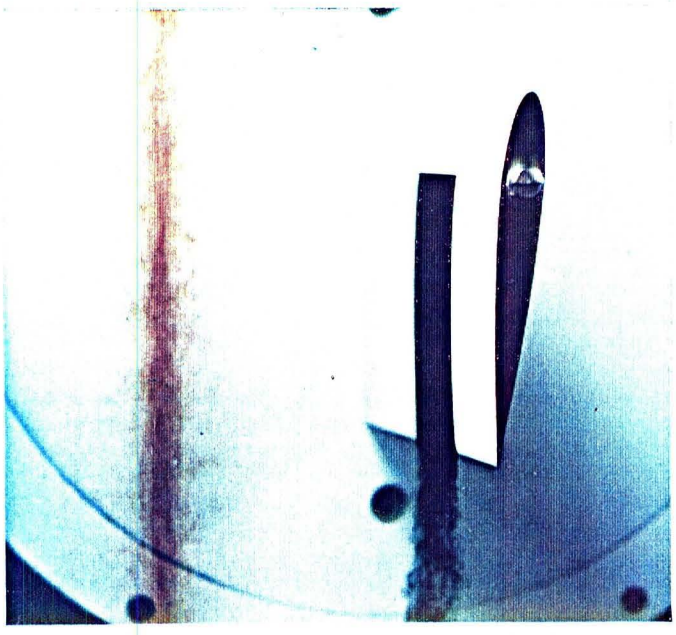

(a) Sideview, d = 0.75 c.

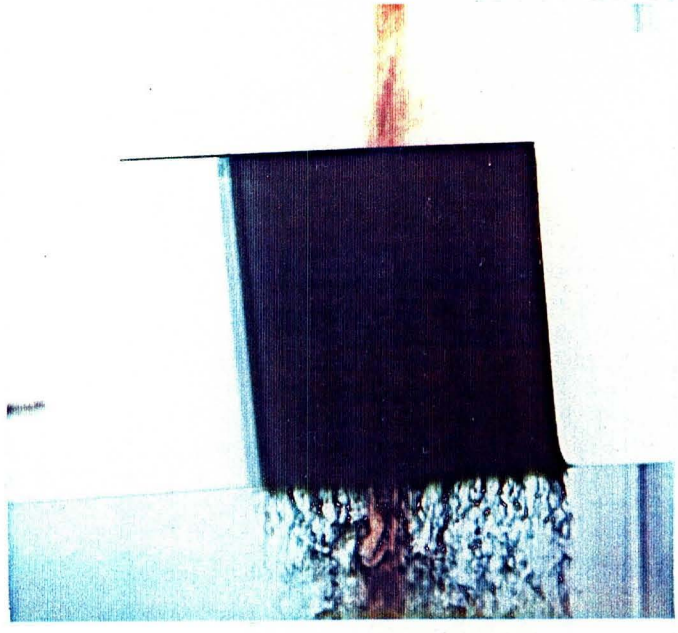

(b) Plan view, d = 0.75 c.

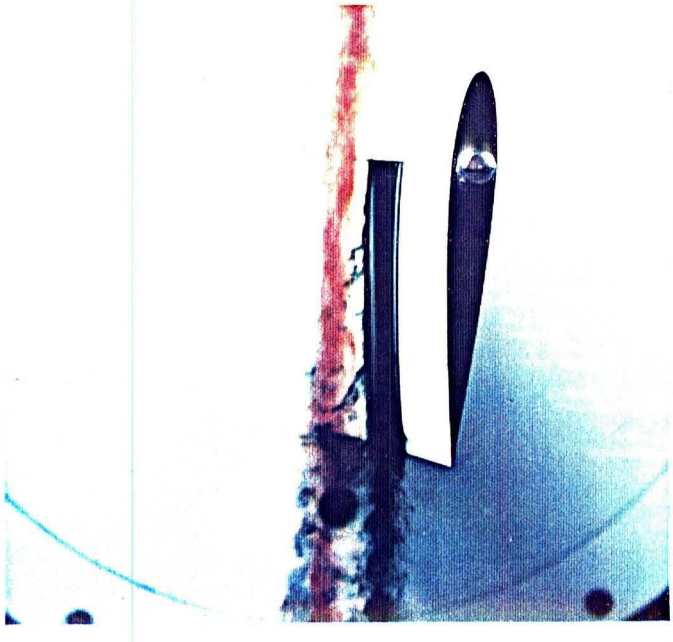

(c) Side view, d = 0.1 c.

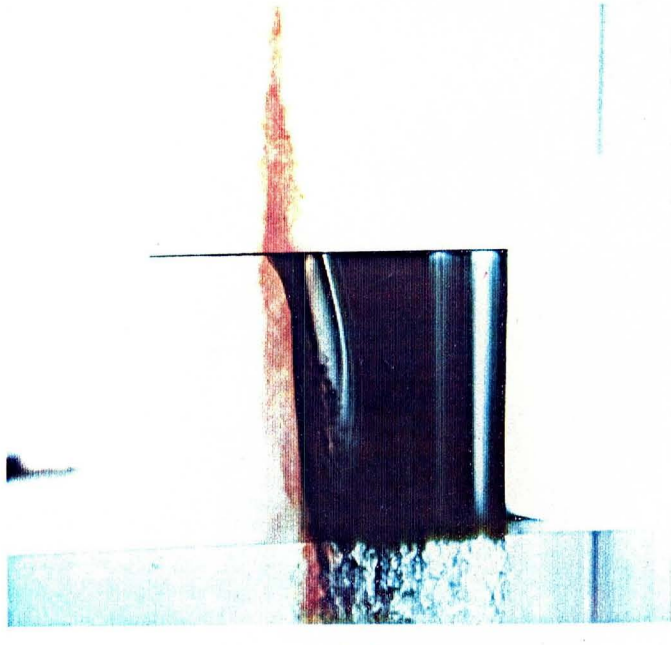

(d) Plan view, d = 0.1 c.

Figure 4.- Simultaneous views of interaction, $\alpha = -5°$.

Plate I

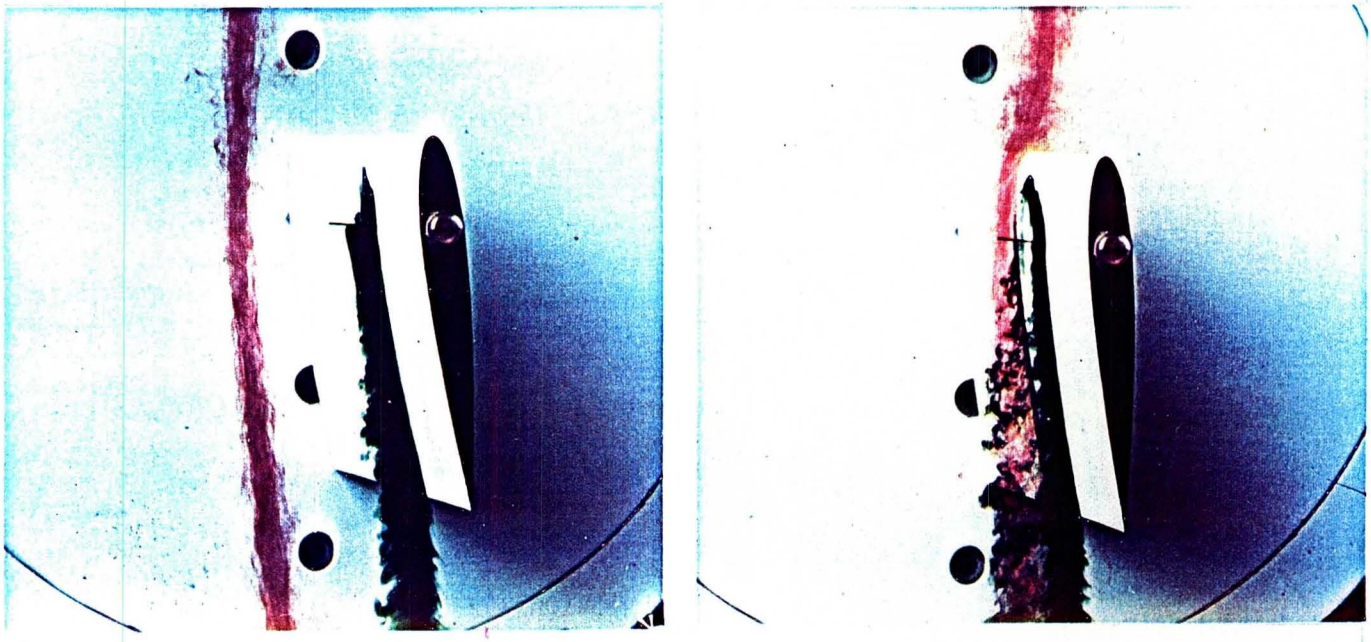

(a) d = 0.6 c.

(b) d = -0.1 c.

Figure 5.- Oblique view of interaction, $\alpha = 5°$.

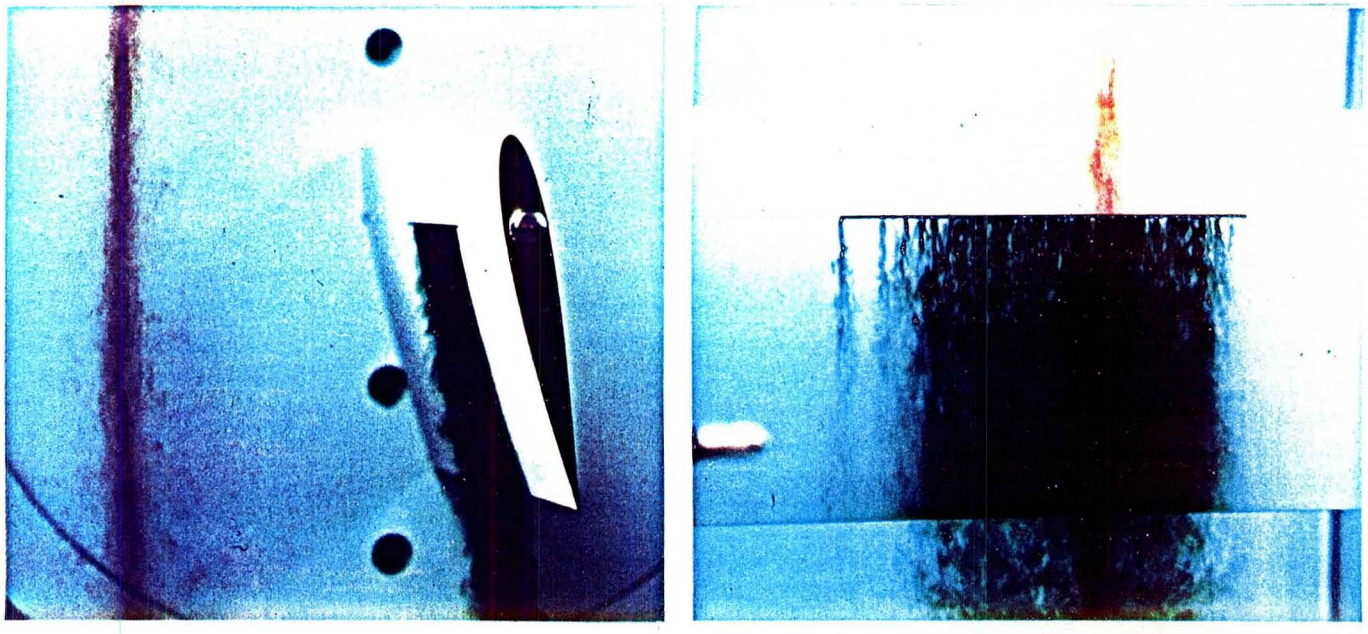

(a) Side view, d = 0.75 c.

(b) Plan view, d = 0.75 c.

Figure 6.- Simultaneous views of interaction, $\alpha = 10°$.

Plate II

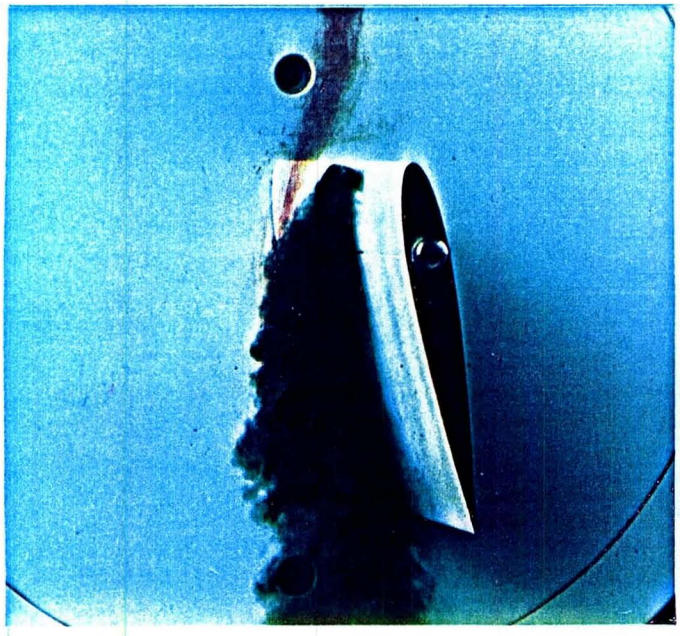

(c) Side view, d = -0.15 c.

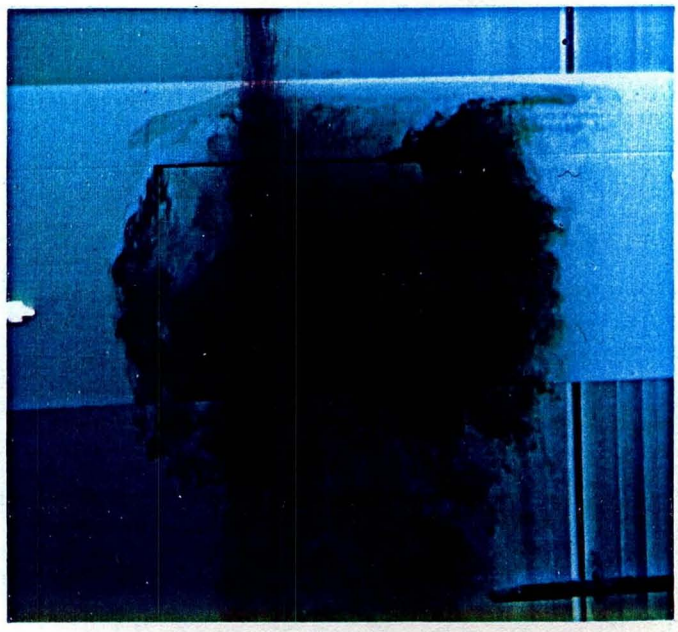

(d) Plan view, d = -0.15 c.

Figure 6.- Concluded.

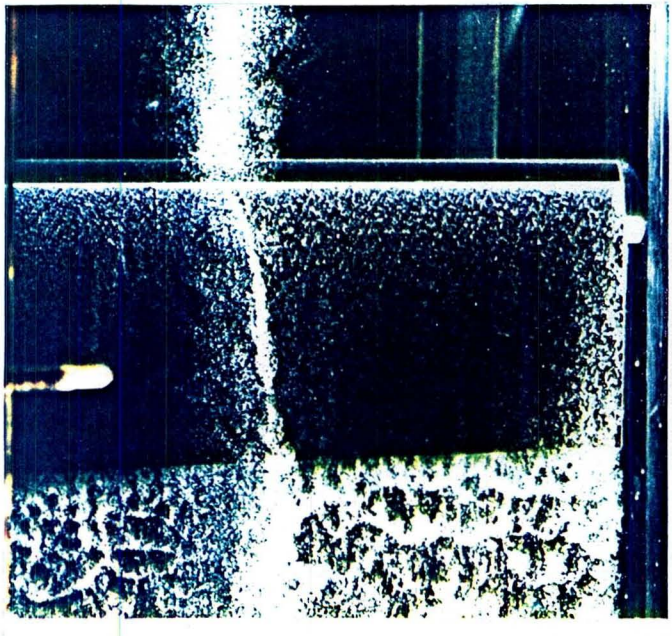

Figure 7.- Plan view of interaction using hydrogen bubbles technique, $\alpha = 0^{\circ}$.

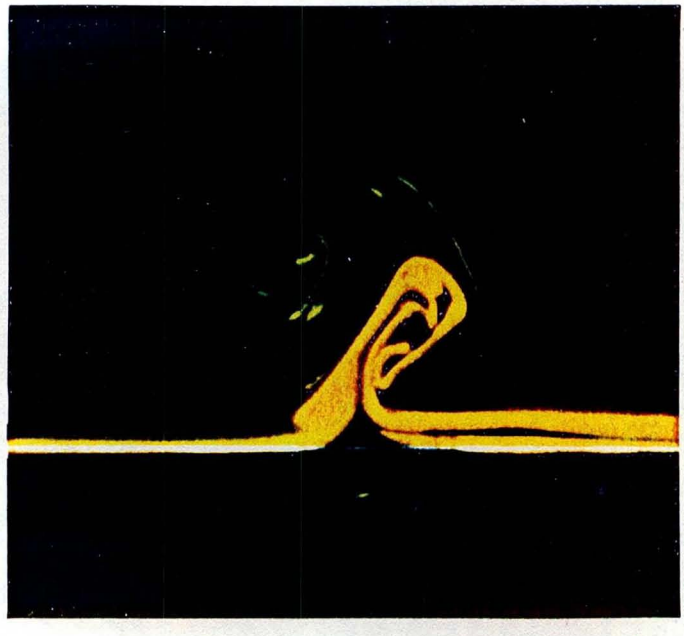

Figure 10.- Cross-sectional view of interaction showing the scondary vortex, $\alpha = 0^{\circ}$, photograph courtesy of B. G. McLachlan.

Plate III

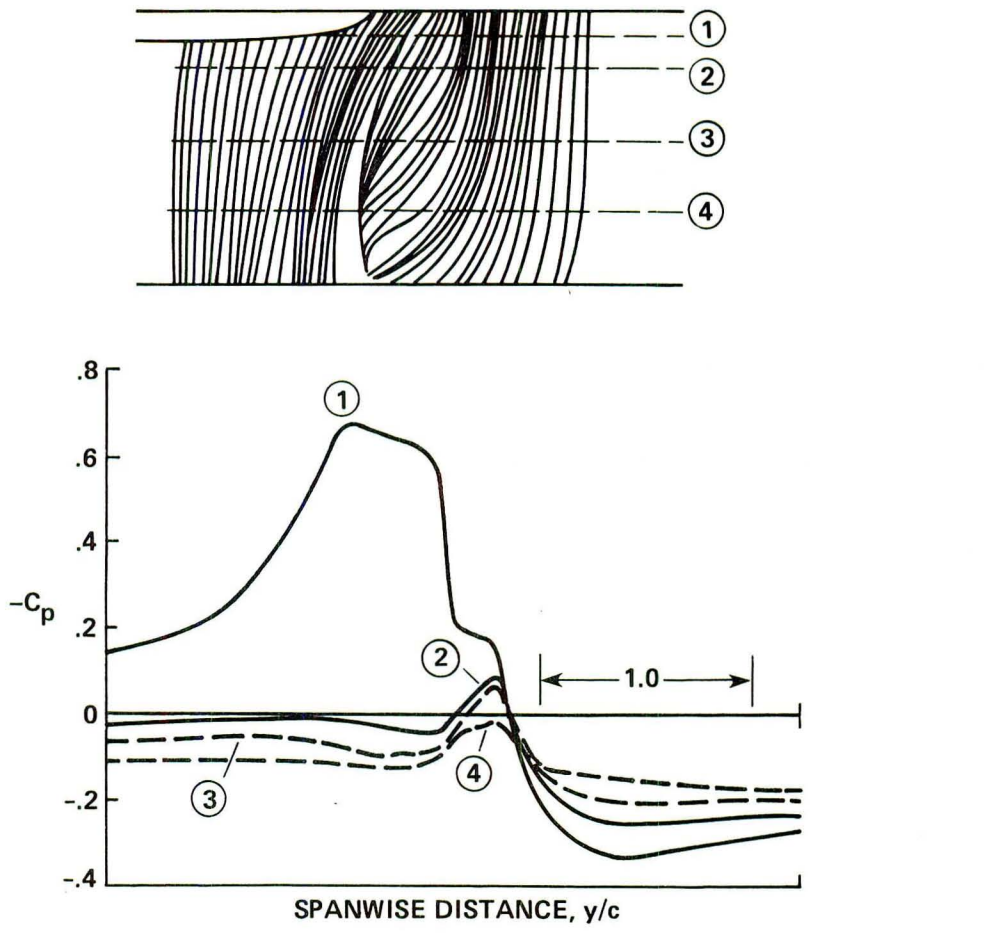

Figure 8.- Oil-flow pattern schematic and spanwise pressure distributions (d/c = 0.2), from Patel and Hancock (1974).

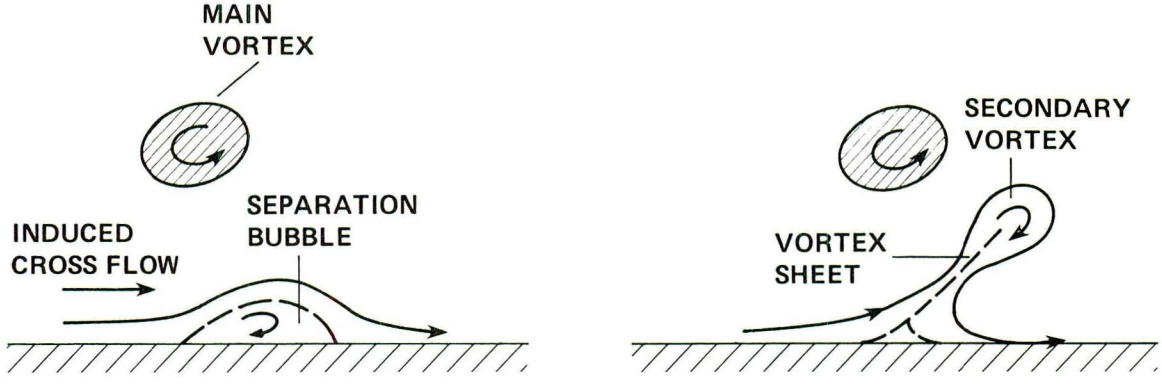

Figure 9.- Conjectural interpretation of total-head surveys, from Harvey and Perry (1972).

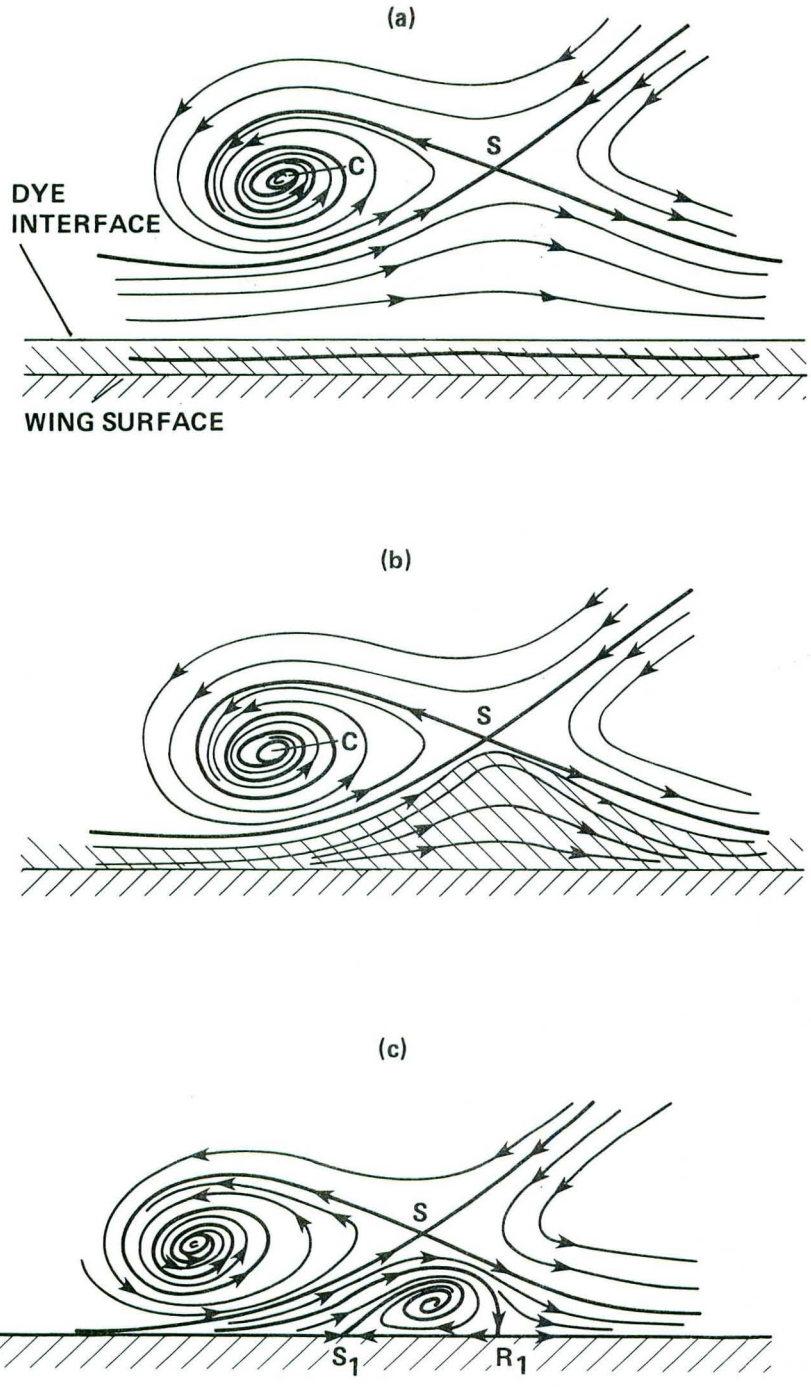

Figure 11.- Conjectured streamline patterns for vortex/wing interaction as vortex moves closer to the wing surface, for $-5° < \alpha < 5°$. (a) Vortex induces cross flow in boundary layer. (b) Vortex causes boundary layer flow to lift up. (c) Vortex causes secondary separation.

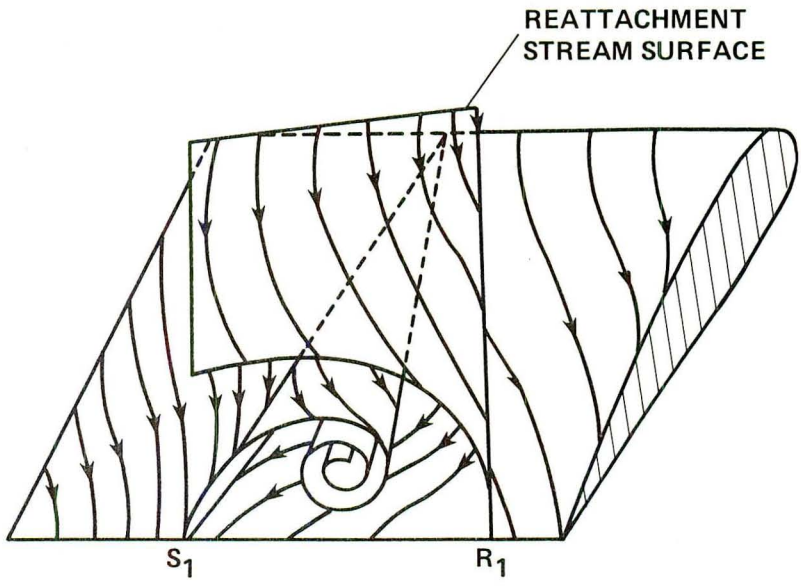

(a)

Figure 12a.- Perspective view of secondary separation shown in figure 11c.

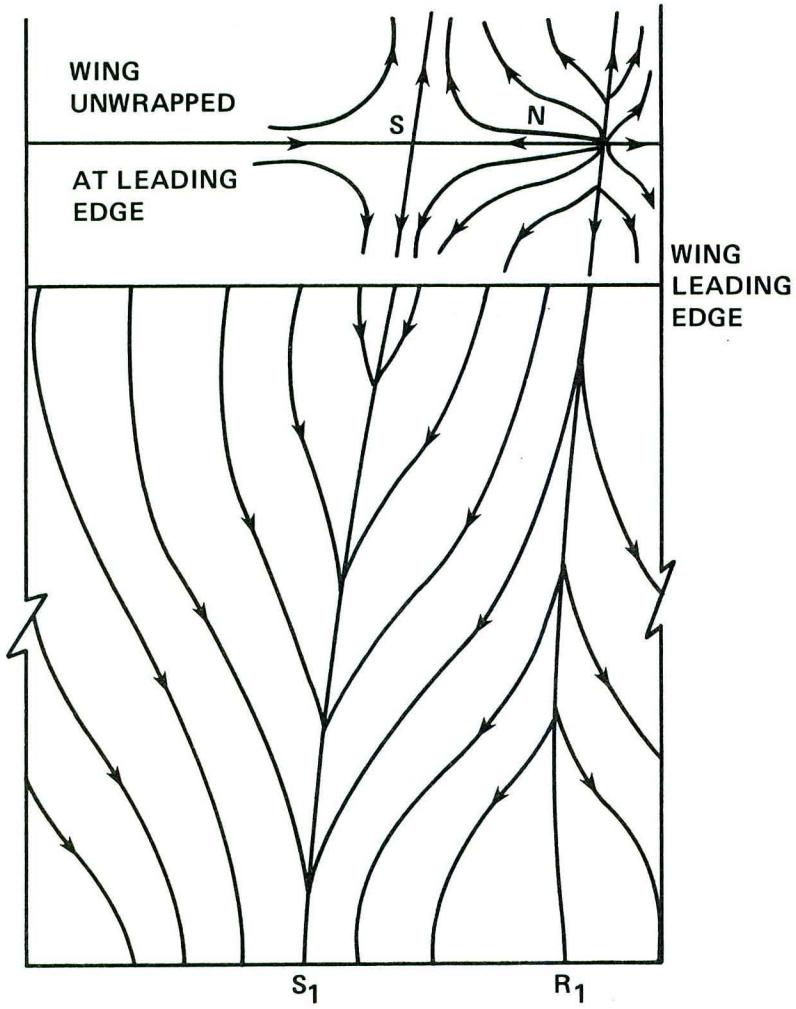

(b)

Figure 12b.- Surface flow pattern with secondary separation corresponding to figure 12a.

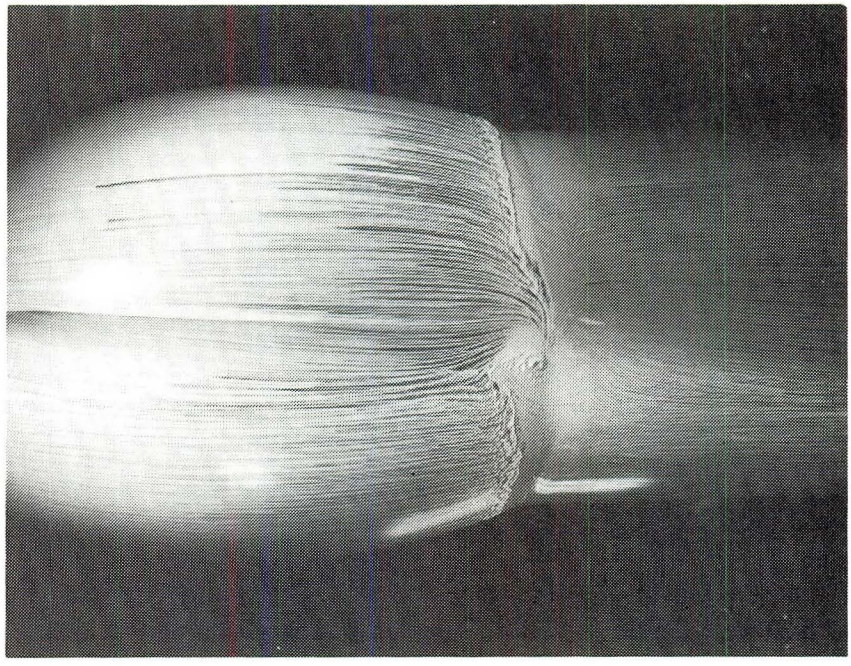

Figure 13.- Oil-flow visualization of a longitudinal vortex interacting with a separated boundary layer on a bump model.

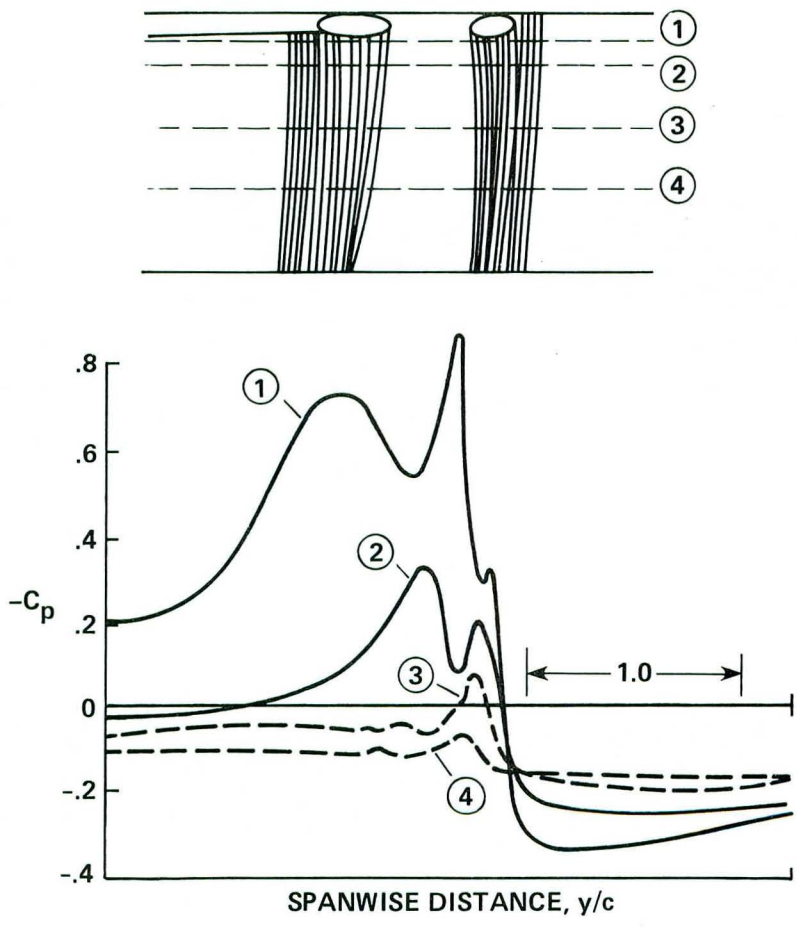

Figure 14.- Oil-flow pattern schematic and spanwise pressure distributions (d/c = 0.0), from Patel and Hancock (1974).

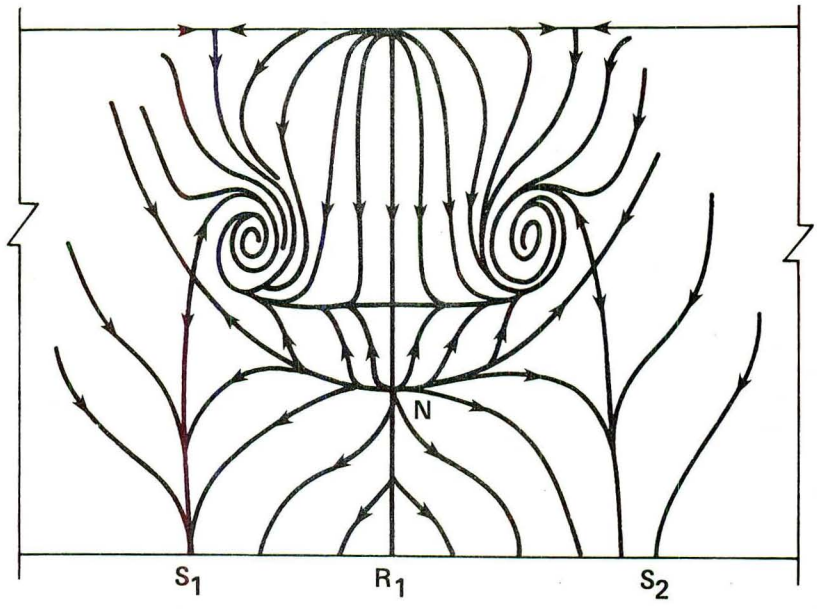

(a)

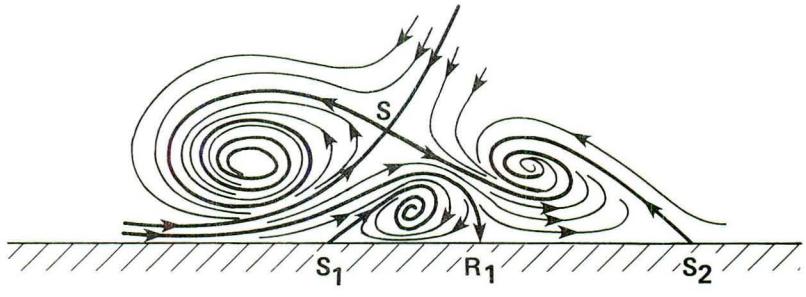

(b)

Figure 15.- Conjectured surface flow and cross-flow patterns for $\alpha = 5°\text{-}10°$. (a) Surface flow pattern. (b) Cross-flow pattern.

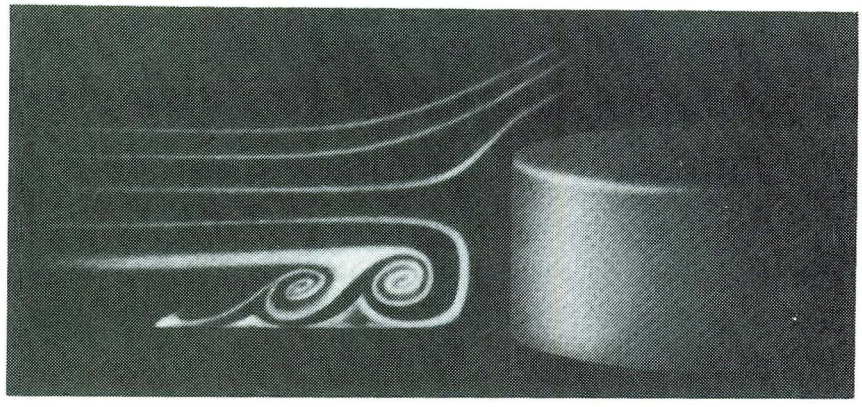

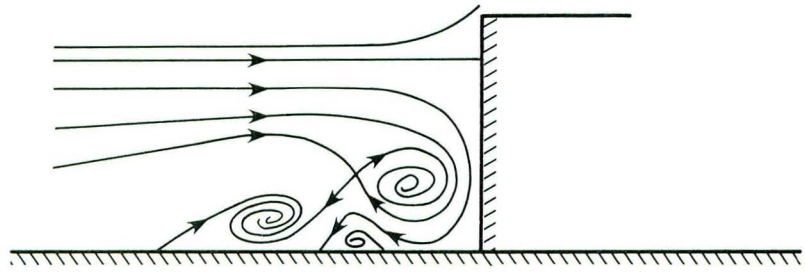

Figure 16.- Artist's sketch of flow upstream of a protuberance, from Tobak (1973). Original photograph in Thwaites (1960).

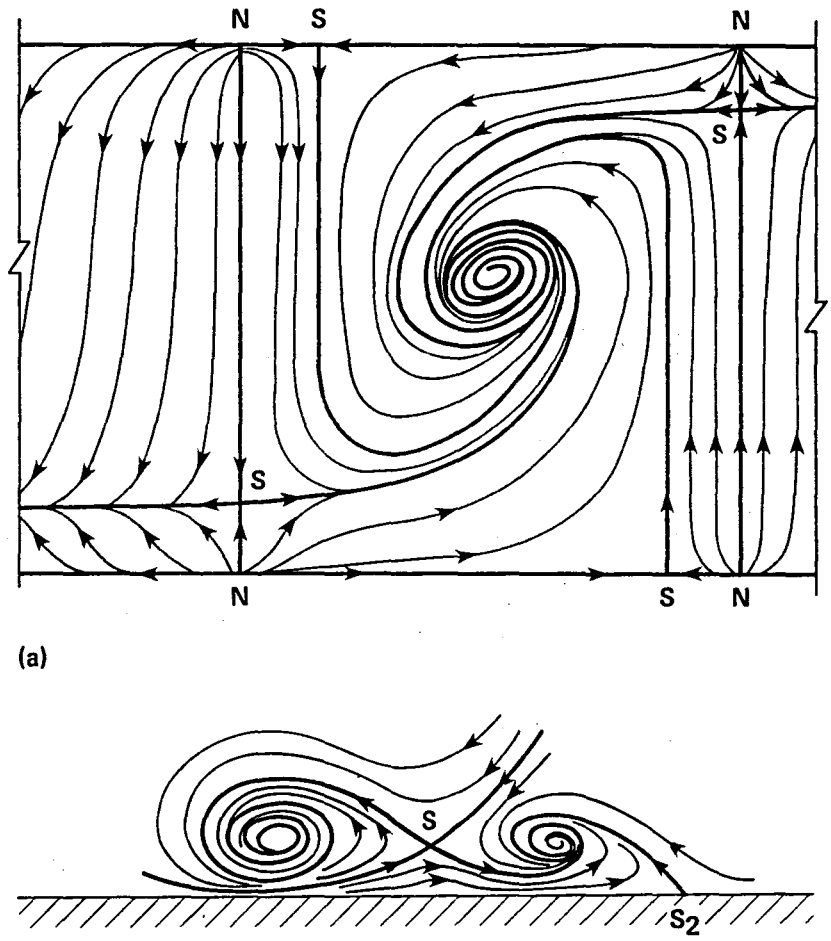

Figure 17.- Conjectured surface flow and cross-flow patterns for $\alpha = 10°$. (a) Surface flow pattern. (b) Cross-flow pattern.

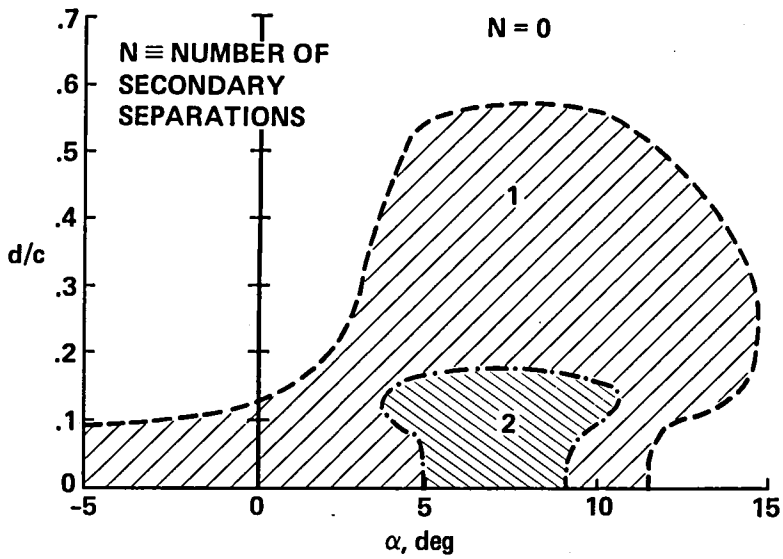

Figure 18.- Topography of separation lines.

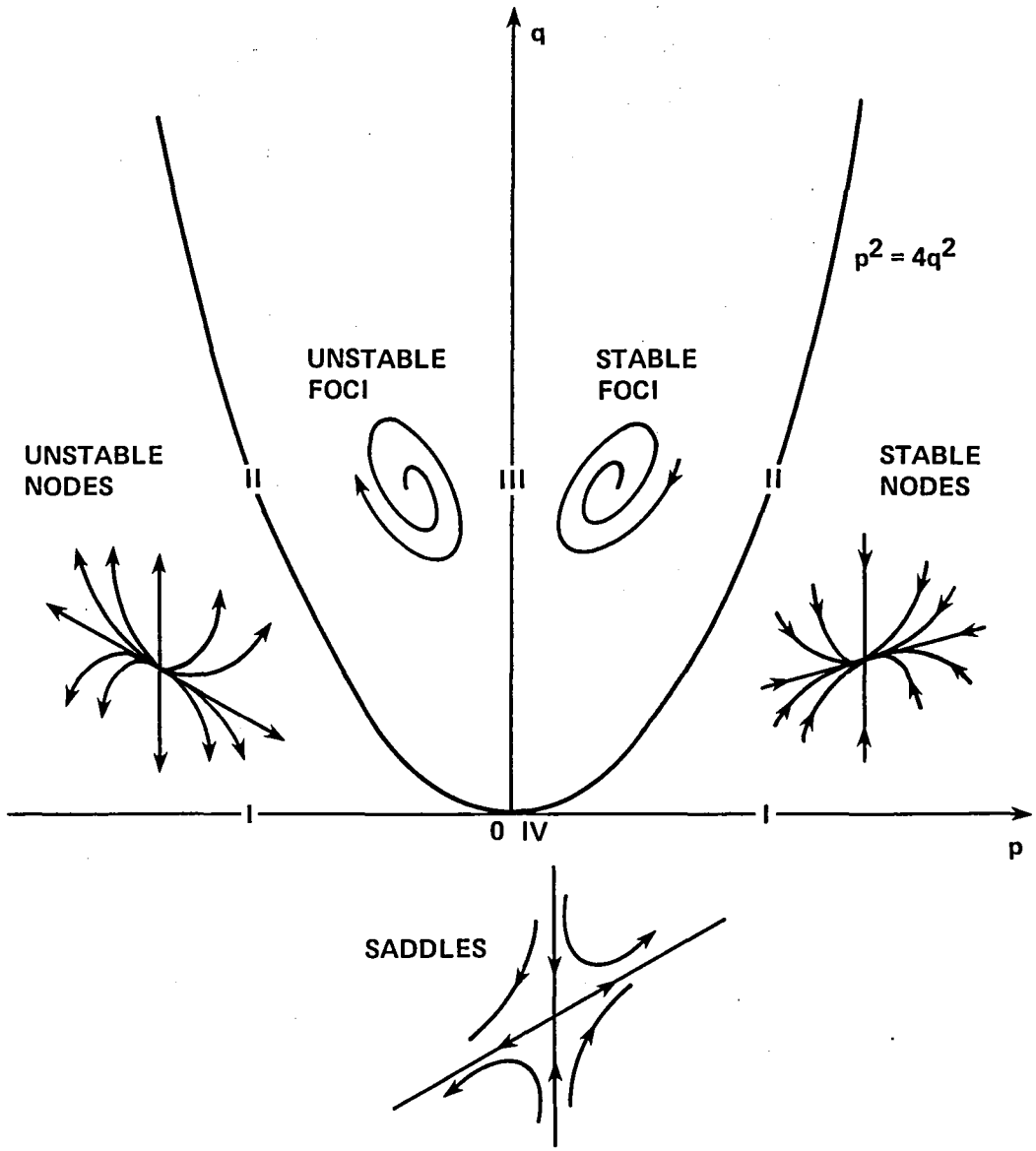

Figure A.1.- p - q chart showing classification of critical points.

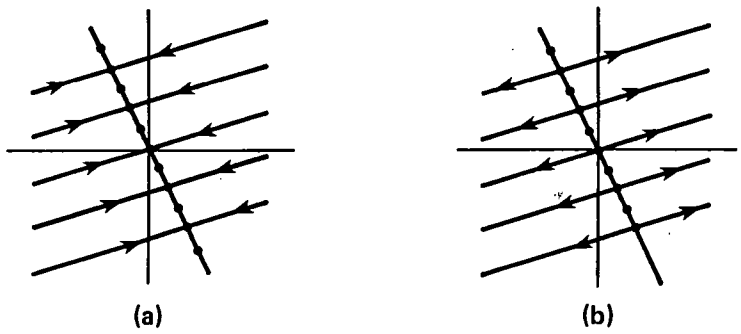

CASE I (a) NEUTRALLY STABLE; (b) UNSTABLE

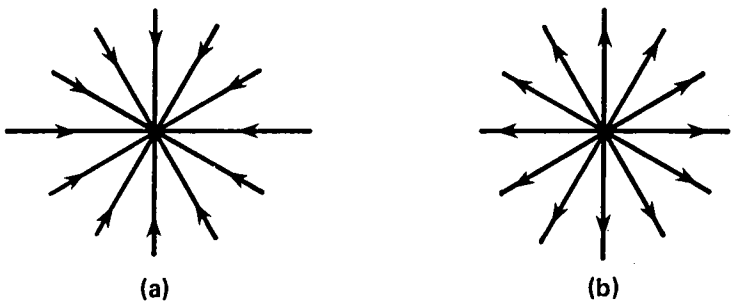

CASE II STAR NODES: (a) STABLE (b) UNSTABLE

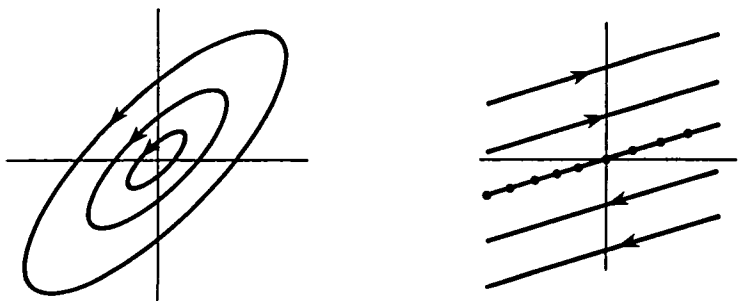

CASE III CENTER CASE IV

Figure A.2.- Classification of degenerate critical points. Roman numerals correspond to those shown in figure A.1.

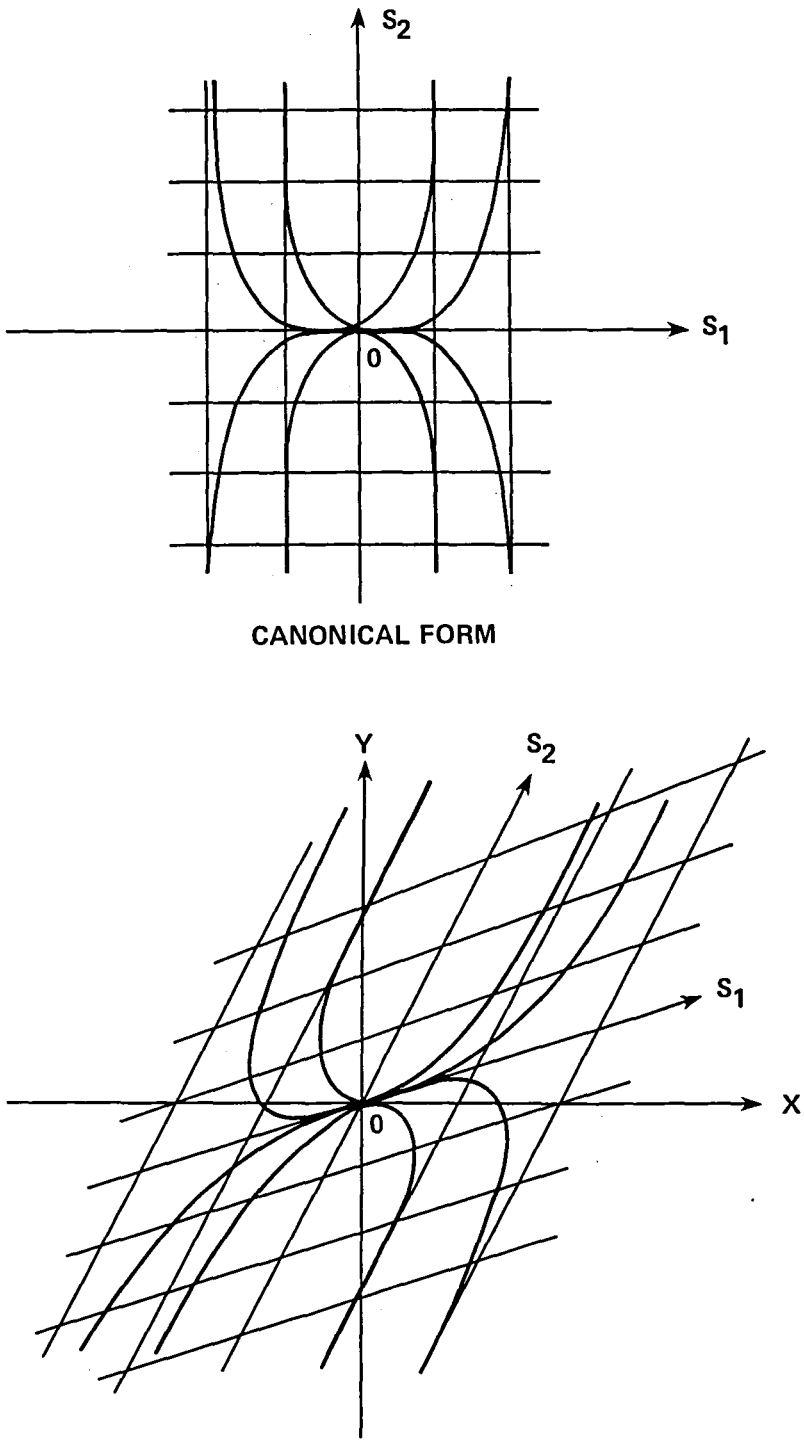

(a) Phase plane portrait of a node.

Figure A.3.- Demonstration of an affine transformation from X,Y plane to S_1, S_2 plane (from Perry and Fairlie, 1974).

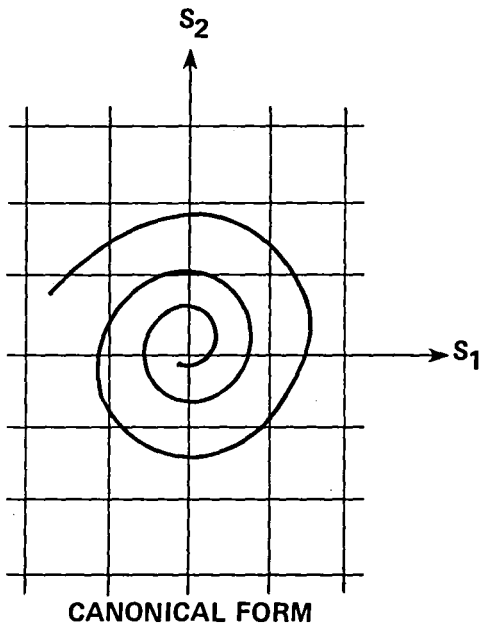

CANONICAL FORM

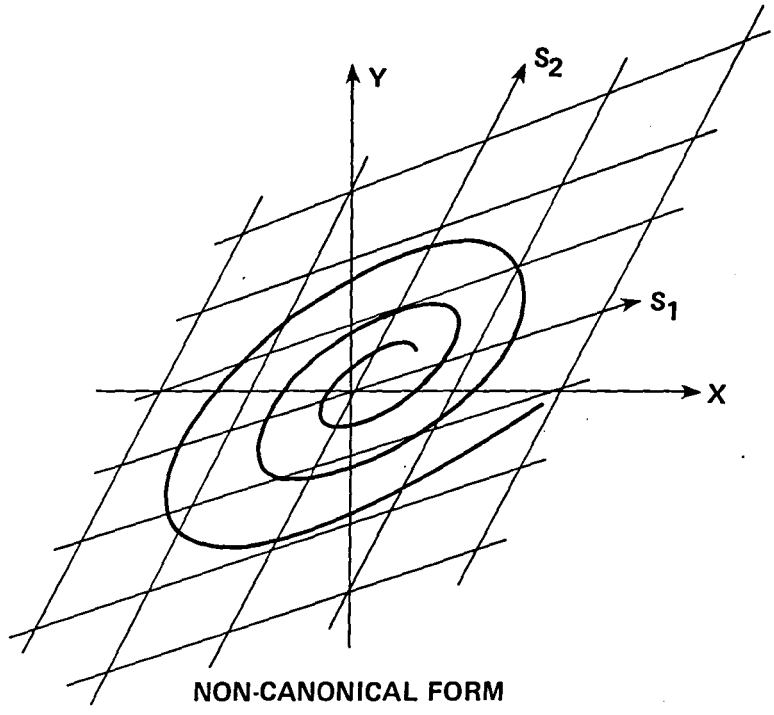

NON-CANONICAL FORM

(b)

(b) Phase plane portrait of a focus.

Figure A.3.- Concluded.

1. Report No.	2. Government Accession No.	3. Recipient's Catalog No.
NASA TM-86656		

4. Title and Subtitle	5. Report Date
FLOW VISUALIZATION STUDY OF A VORTEX/WING INTERACTION	November 1984
	6. Performing Organization Code

7. Author(s)	8. Performing Organization Report No.
R. D. Mehta and T. T. Lim	85013
	10. Work Unit No.

9. Performing Organization Name and Address	11. Contract or Grant No.
Ames Research Center Moffett Field, Calif. 94035	
	13. Type of Report and Period Covered
12. Sponsoring Agency Name and Address	Technical Memorandum
National Aeronautics and Space Administration Washington, D.C. 20546	14. Sponsoring Agency Code 505-31-11

15. Supplementary Notes

Point of Contact: Rabi D. Mehta, Ames Research Center, Moffett Field, CA 94035, (415) 965-5862 or FTS 448-5862

16. Abstract

A flow visualization study in water has been completed on the interaction of a streamwise vortex with a laminar boundary layer on a two-dimensional wing. The vortex was generated at the tip of a finite wing at incidence, mounted perpendicular to the main wing, and having the same chord as the main wing. The Reynolds number based on wing chord was about 5×10^4. Two different visualization techniques were used. One involved the injection of two different colored dyes into the vortex and the boundary layer. The other technique utilized hydrogen bubbles as an indicator. In this study, the position of the vortex was varied in a direction normal to the wing. The angle of attack of the main wing was varied from -5° to +12.5°. It was found that the vortex induced noticeable cross flows in the wing boundary layer from a distance equivalent to 0.75 chords. When very close to the wing, the vortex entrained boundary layer fluid and caused a cross flow separation which resulted in a secondary vortex. In certain cases, two secondary vortices of opposite sign were induced and, in the right circumstances, asymmetric primary separation was also obtained on the main wing. The visual observations are also analyzed and discussed with respect to the critical point theory.

17. Key Words (Suggested by Author(s))	18. Distribution Statement
Vortex Wing Interaction Secondary flow Flow visualization	Unlimited Subject Category - 02

19. Security Classif. (of this report)	20. Security Classif. (of this page)	21. No. of Pages	22. Price*
Unclassified	Unclassified	43	A03

*For sale by the National Technical Information Service, Springfield, Virginia 22161

End of Document